

# Solar Hydrogen

Zhongxiao Li, Shi Fang, Haiding Sun,\* Ren-Jei Chung,\* Xiaosheng Fang,\* and Jr-Hau He\*

Hydrogen, produced through a zero-pollution, sustainable, low-cost, and high-efficiency process, is regarded as the “ultimate energy” of the 21st century. Solar water-splitting techniques have immense potential to make the idea a reality. Two promising approaches, photovoltaic-electrolysis (PV-EC) and photoelectrochemistry (PEC), have demonstrated solar-to-hydrogen conversion efficiency over 10%, which is the minimum required for competitively priced, large-scale systems. Extensive studies of PV-EC and PEC devices reported within the past five decades show increasing design complexity. To accurately describe the gap between laboratory research and practical application, the basic principles and concepts of PV-EC and PEC are elaborated and clarified. The history of these developments is systematically summarized, and a comprehensive techno-economic analysis of PV-EC and PEC solar hydrogen production of 10 000 kg H<sub>2</sub> day<sup>-1</sup> is performed. The analysis shows that no solar hydrogen system is currently competitive with production methods based on fossil fuels, but the development of high-efficiency water-splitting electrolyzers with cost-competitive components (especially for cation/anion exchange membranes) can accelerate progress.

become essential for all humanity.<sup>[1]</sup> Hydrogen is an alternative for the next generation of clean energy, especially in fuel developments with paths from high to low carbon content and low to high energy density. Hydrogen is free of carbon and when used releases no greenhouse gases or harmful substances. Hydrogen also has a gravimetric heating value (141.9 MJ kg<sup>-1</sup>) which is much higher than that of traditional fuels, such as petrol (47.5 MJ kg<sup>-1</sup>) and natural gas (55.5 MJ kg<sup>-1</sup>).<sup>[2]</sup> However, hydrogen production is not environmentally friendly; where over 90% originates from fossil fuels, emitting a large amount of CO<sub>2</sub> and pollutants.<sup>[3]</sup> Hence, “green hydrogen” processes with zero-pollution, sustainability, and high efficiency are a focus of the 21st century.

In combination with solar energy, “green hydrogen” production is an opportunity.<sup>[4]</sup> A few technologies converting sunlight into hydrogen have been developed

over the past century. However, low solar-to-hydrogen (STH) efficiencies restrict large-scale development. Recently, photovoltaic-electrolysis (PV-EC) and photoelectrochemical (PEC) systems have realized an STH efficiency of over 10% at laboratory scale,<sup>[5]</sup> which indicates scale-up potential.<sup>[6]</sup> Meanwhile, PEC technology has been demonstrated with numerous devices in the past half-century; such as “artificial leaf,”<sup>[7]</sup> “integrated PEC,”<sup>[5a]</sup> and “integrated PV-EC.”<sup>[8]</sup> To develop green hydrogen further, we clarify the differences between PV-EC and PEC concepts, review the developments of both processes, summarize past studies, and estimate their potential for scale-up.

In this review, we elaborate on the fundamental principles of PEC and PV-EC systematically and clarify their classifications. Then, we discuss the representative research on PV-EC and PEC chronologically, presenting the development trend. One of the essential aspects of this review is a techno-economic analysis. Except for PV-EC, a large-scale PEC hydrogen production system (10 000 kg H<sub>2</sub> day<sup>-1</sup>) with a semiconductor-liquid junction (SLJ) is designed and analyzed. Conclusions and potential future developments for PV-EC and PEC are summarized. Note that this review is restricted to hydrogen production. The reader can refer to the literature related to the distribution, storage, and utilization of hydrogen,<sup>[9]</sup> which are essential to constructing a “hydrogen society in the future.”

## 1. Introduction


Facing global energy and environmental pollution crises, developing green, sustainable, and low-cost energy has

Z. X. Li, J.-H. He  
Department of Materials Science and Engineering  
City University of Hong Kong  
Kowloon, Hong Kong SAR 999077, China  
E-mail: jrhouhe@cityu.edu.hk

S. Fang, H. Sun  
School of Microelectronics  
University of Science and Technology of China  
Hefei, Anhui 230026, China  
E-mail: haiding@ustc.edu.cn

R.-J. Chung  
Department of Chemical Engineering and Biotechnology  
National Taipei University of Technology (Taipei Tech)  
Taipei 10608, Taiwan  
E-mail: rjchung@ntut.edu.tw

X. S. Fang  
Department of Materials Science  
State Key Laboratory of Molecular Engineering of Polymers  
Fudan University  
Shanghai 200433, China  
E-mail: xshfang@fudan.edu.cn

 The ORCID identification number(s) for the author(s) of this article can be found under <https://doi.org/10.1002/aenm.202203019>.

DOI: 10.1002/aenm.202203019

## 2. Fundamentals of PEC and PV-EC Solar Hydrogen Systems

### 2.1. Principle and Mechanism

There are three fundamental requirements for any solar water-splitting system:<sup>[10]</sup> First, sunlight must be efficiently absorbed to produce excited electron states in the light-absorbing material. Second, the photoexcited electrons and holes must be separated in space to prevent their recombination. Third, the photoexcited charges must be energetically and kinetically able to perform overall water-splitting reaction, an energetically uphill reaction requiring a standard free-energy change  $\Delta G^0 = +237 \text{ kJ mol}^{-1}$  or a potential of 1.23 eV per electron.

**Figure 1** presents a typical SLJ formation process in a PEC water-splitting device with an n-type photoanode and one standard metallic electrode.<sup>[11,12]</sup> In the dark, when an n-type semiconductor photoanode is in contact with the electrolyte, the electrons will flow between the semiconductor and the electrolyte due to the built-in voltage ( $V_{BI}$ ), the differences between the Fermi energy ( $E_F$ ) of the semiconductor and the electrochemical potential of a redox couple  $E^0$  (e.g.,  $\text{O}_2/\text{H}_2\text{O}$ ) in an acid electrolyte (Figure 1a). Charge transfer results in band bending near the SLJ and provides an interfacial electric field to separate the photogenerated charge carriers at equilibrium (Figure 1b). Under light illumination, electrons ( $e^-$ ) will be excited by high-energy photons ( $h\nu > E_g$ ) from the valence band (VB) to the conduction band (CB), where holes ( $h^+$ ) are left in the VB of the n-type semiconductor. The photovoltage ( $V_{ph}$ ) arises simultaneously from splitting electron and hole quasi-Fermi levels (Figure 1c). Then, the interfacial electric field will drive the minority charge carriers ( $h^+$ ) to reach the surface of the semiconductor for the oxygen evolution reaction (OER), while the majority charge carriers (electrons) will be consumed by the hydrogen evolution reaction (HER) at a counter electrode.

A PEC cell requires two electrodes (an anode for the oxidation reaction and a cathode for the reduction reaction). At least one of the electrodes is a semiconductor (n-type for photoanode and p-type for photocathode) designed to absorb the sunlight and split water directly at the surface (**Figure 2a**). Considering the high thermodynamic potential and multielectron kinetic process, not all PEC cells can drive the water-splitting reaction

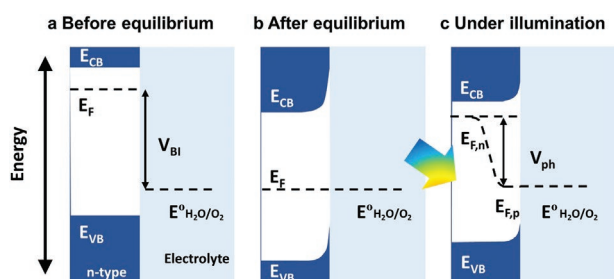


**Figure 1.** The SLJ photoelectrode device concept illustrated for an n-type semiconductor photoanode. a) Before equilibrium between the semiconductor and the electrolyte. b) After equilibrium without illumination. c) Quasi-equilibrium under illumination. Reproduced with permission.<sup>[11]</sup> Copyright 2017, Elsevier.

only under sunlight illumination. Therefore, some kinds of PEC cells require an additional electric power supply to provide the energy difference when illuminating, called assisted/biased PEC cells. Others that can drive the reaction directly by solar energy are called unassisted PEC cells. This review will be conducted based on unassisted PEC cells in the following section. A PEC cell with one single-junction semiconductor photoelectrode and one standard metallic electrode can be envisioned. The bandgap energy ( $E_g$ ) of the semiconductor should be 1.6–2.4 eV, and the conduction band-edge energy ( $E_{cb}$ ) and valence band-edge energy ( $E_{vb}$ ) should straddle the electrochemical potentials  $E^0$  ( $\text{H}^+/\text{H}_2$ ) and  $E^0$  ( $\text{O}_2/\text{H}_2\text{O}$ ). Therefore, identifying a single semiconductor that can both develop sufficient photovoltage and harvest a large portion of the solar spectrum is an ongoing and complex challenge. On the other hand, two semiconductors with different  $E_g$  can be constructed for both electrodes in a tandem PEC cell configuration resulting from the fact that semiconductors can transmit photons with energy less than their  $E_g$ .<sup>[14]</sup> A typical schematic called photoanode–photocathode (or PEC–PEC) tandem cell is presented in Figure 2b.<sup>[4b]</sup> A photoanode with large  $E_g$  absorbs high-energy incoming photons and transmits the remainder to the photocathode below. As such, photogenerated electrons in the CB of the photoanode will be combined with holes in the VB of the photocathodes through the wires. The minority charge carriers (electrons in the photocathode and holes in the photoanode) are still used for HER and OER at the respective SLJs. The photoanode–photocathode tandem configuration allows absorption of a broader spectrum as more low-energy photons will be used compared to the one semiconductor PEC configuration with the same area. At the same time, the photovoltage of the tandem cells is the sum of  $V_{ph}$  of the two photoelectrodes, which provide enough photovoltage for water splitting.

Except for SLJs, buried junctions where the driving force comes from the built-in potential from the interface of solid-state materials rather than the semiconductor-liquid have been demonstrated to be powerful methods to construct an effective PEC cell.<sup>[4b,15]</sup> Figure 2c depicts two buried p–n junctions connected in series for a PEC construction called buried-junction PEC cell. In contrast to the photoanode–photocathode tandem cell, the majority carriers, rather than the minority carriers, are injected from the solid-state photoelectrode into the electrolyte to conduct water reduction/oxidation. Another feasible strategy for PEC water splitting through the combination of SLJ and buried junction is named photoelectrode-photovoltaic (PEC-PV) cell.<sup>[16]</sup> As shown in Figure 2d, the majority carriers generated (electrons) in the buried p–n junction reduce protons in the electrolyte, and minority holes produced in the n-type photoelectrode oxidize water at its surface. Typically, two (photo)electrodes are electrically connected by an external wire called “wired” PEC cells (Figure 2). There is another “wireless” cell design where both the photoanode and photocathode mentioned above are directly adjoined back-to-back, known as “artificial leaf.”<sup>[7,15,17]</sup>

Compared to the PEC devices, where a light absorber is immersed in the electrolyte, the PV-EC devices employ a separate function of light absorption and electrolysis. Specifically, two well-established technologies, PV and EC, are combined. Solar energy is transformed into electrical power by PV devices

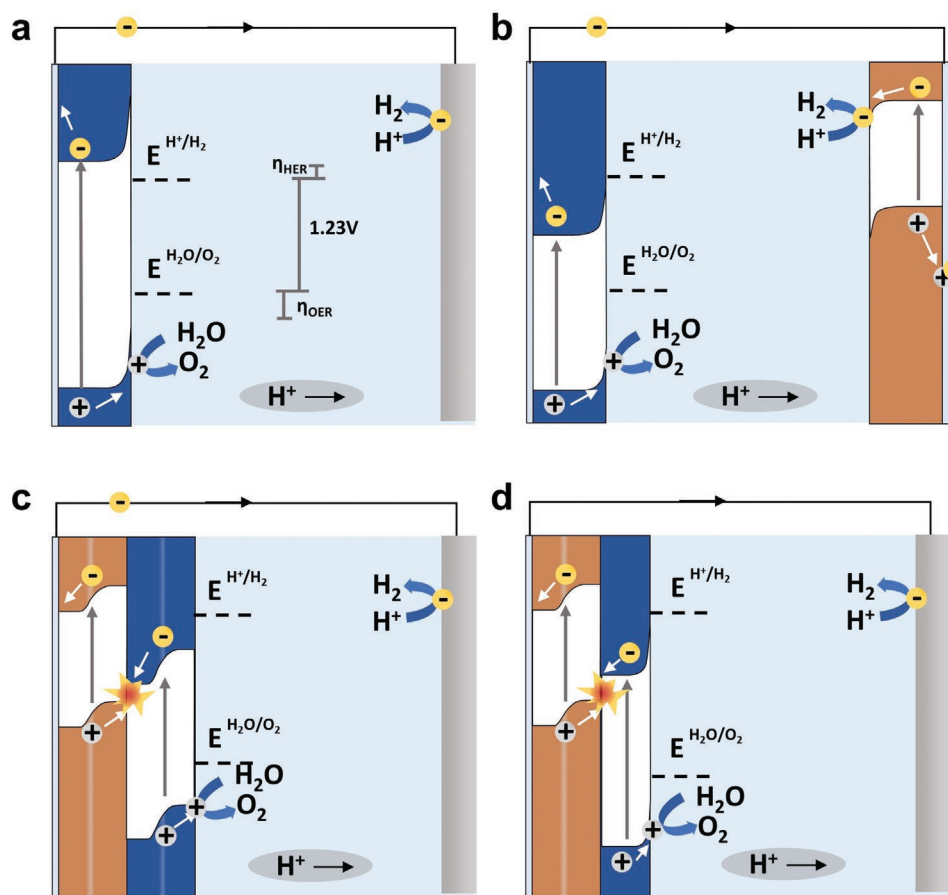


**Figure 2.** Energy diagrams for four types of PEC devices. a) A single band gap photoanode with a metal cathode. b) A photoanode–photocathode PEC configuration with n-type and p-type photoelectrodes electrically connected in series. c) A buried-junction PEC configuration with two p–n PV cells integrated and wired with a metal cathode. d) A photoelectrode-photovoltaic PEC configuration that photoanode is in series with an integrated p–n PV cell to provide additional bias and connect to a metal cathode. Reproduced with permission.<sup>[13]</sup> Copyright 2010, American Chemical Society.

and then transports to the electrolyzers through the wires for water splitting (Figure 3a). The PV and EC can be treated as two independent parts, which gives more freedom to be modularized and optimized. However, a high photovoltage ( $\approx 1.6\text{--}1.7\text{ V}$ ) is required even with state-of-the-art electrocatalysts. In addition

to using a multijunction solar cell similar to the tandem configuration in a PEC cell,<sup>[18]</sup> the interconnection of single-junction solar cells in series is the most common method for PV-EC construction (Figure 3a).<sup>[19]</sup> Alternatively, the PV-EC device can be arranged as an integrated configuration instead of a separate one. More details about the integrated PV-EC (Figure 3b) will be discussed in Section 3. To further distinguish the different classifications of PV-EC devices and PEC cells, all configuration types are summarized in Figure S1 in the Supporting Information. The position of the light absorber, rather than the physical principles,<sup>[20]</sup> determines the specific categories. Therefore, although some literature discusses “integrated PEC cells,” in which a photo-absorber/solar cell is totally outside the electrolyzer by coating the conducting layer,<sup>[5a,21]</sup> we prefer to classify them into “integrated PV-EC” in the following sections.

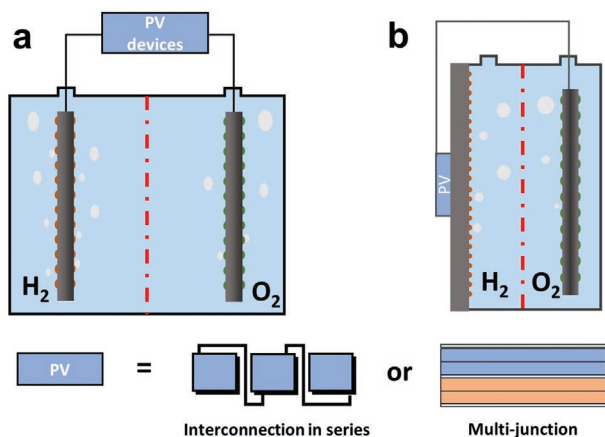


**Figure 3.** Schematic of two types of PV-EC devices/systems: a) Traditional PV-EC. b) Integrated PV-EC.

## 2.2. STH Conversion Efficiency

Under the premise of essential operation, the performance of a solar hydrogen production device/system should be quantified by which kinds of devices/systems can be compared reliably. The STH efficiency ( $\eta_{\text{STH}}$ ) is a standard parameter defined as

the amount of hydrogen energy produced against the incident solar energy

$$\eta_{\text{STH}} (\%) = \frac{\text{H}_2 \text{ energy produced}}{\text{Solar energy input}} = \frac{\text{Rate of H}_2 \text{ production (mol s}^{-1}) \times \Delta G_{\text{H}_2} \text{ (kJ mol}^{-1})}{P_{\text{sun}} \text{ (mW cm}^{-2}) \times S \text{ (cm}^2)} \quad (1)$$

where  $\Delta G_{\text{H}_2}$  is the Gibbs free energy of hydrogen molecules (at 25 °C  $\Delta G = 237 \text{ kJ mol}^{-1}$ );  $P_{\text{sun}}$  is the standard solar irradiation generated with the Air Mass 1.5 global (AM 1.5 G) filter (100 mW cm<sup>-2</sup>), i.e., one sun illumination.

For simplicity, the operating photocurrent density ( $J_{\text{op}}$ ) is measured instead of the rate of H<sub>2</sub> production in many cases

$$\eta_{\text{STH}} (\%) = \frac{J_{\text{op}} \text{ (mA cm}^{-2}) \times 1.23 \text{ (V)} \times \eta_{\text{F}}}{P_{\text{sun}} \text{ (mW cm}^{-2})} \quad (2)$$

where  $\eta_{\text{F}}$  is the Faradaic efficiency of H<sub>2</sub> or O<sub>2</sub> production and  $J_{\text{op}}$  is based on the area of the light absorber (semiconductor or solar cells) rather than that of (photo)electrodes.

A theoretical calculation of STH efficiency can provide a baseline of the performance of the solar hydrogen production system. The maximum theoretical efficiency limit for a single semiconductor PEC cell is 11.2% for an  $E_{\text{g}}$  of 2.26 eV, which falls short of the 31% thermodynamic limit, highlighting the significant losses associated with reaction overpotentials.<sup>[22]</sup> Surprisingly, while the conditions and losses specified in a model can lead to a varied maximum predicted STH efficiency, an attractive STH efficiency (at least) over 20% and even up to 30% can be expected with a tandem cell. Recently, detailed balance calculations of practical STH efficiency with more comprehensive estimation showed that the maximum value for a dual-stacked absorber system is  $\approx 27\%$ , with bottom and top photoabsorber band gaps of 1.05 and 1.7 eV, respectively.<sup>[23]</sup> However, the optimum  $E_{\text{g}}$  range for these maximum efficiencies is narrow and still presents a significant challenge for materials development. These values provide a robust reference for an actual device within these ranges of band gaps. In practical measurements, the intersection of two photoelectrodes  $J$ - $V$  curves measured in a three-electrode configuration indicates the  $J_{\text{op}}$  in the unassisted PEC water splitting and is usually used for predicting STH efficiency (Figure 4a).

In a direct connecting PV-EC configuration, the current density and voltage of PV and EC must be identical:  $J_{\text{PV}} = J_{\text{EC}}$  and  $V_{\text{PV}} = V_{\text{EC}}$ . The operational state of the PV-EC devices can be determined as the intersection of the individual  $J$ - $V$  curves of PV and EC. As shown in Figure 4b, the hydrogen energy produced by PV-EC and the losses due to overpotential can be estimated and represented by the blue and orange areas. The discrepancy between the operating (red) and maximum power point (MPP, black) shows the coupling losses (yellow area). The application of a DC-DC converter is an effective method to eliminate coupling loss. Ideally, the converter will allow the operating point of PV-EC to always follow the MPP of the PV cell (Figure 4c). The precise follow increases the current density of PV-EC directly, resulting in more energy stored in hydrogen and higher STH efficiency (dashed line area in Figure 4c).

Although the DC-DC converter can alleviate the coupling losses, the efficiency of the DC-DC converter cannot reach 100% and requires extra cost. Therefore, the efficiency and cost must be traded off carefully in practical applications.

In addition to Equation (1) and Equation (2), the STH efficiency of PV-EC can also be commonly evaluated by

$$\eta_{\text{STH}} = \eta_{\text{PV}} \times \eta_{\text{EC}} \times \eta_{\text{C}} \quad (3)$$

where  $\eta_{\text{PV}}$  and  $\eta_{\text{EC}}$  are the efficiencies of the PV device and the electrolysis process, respectively, and  $\eta_{\text{C}}$  is the coupling arrangement usually caused by losses of mismatching in the direct configuration or auxiliary components, such as DC-DC converters. Assuming  $\eta_{\text{C}}$  is equal to 1, an STH efficiency of 28.7% can be achieved using an efficient bipolar alkaline electrolyzer (73% efficiency) and double-junction (2j) PV cells with  $\approx 41\%$  power conversion efficiency (PCE). Furthermore, a  $\eta_{\text{STH}}$  of 31.8% was obtained using the same efficient electrolyzer and triple-junction (3j) III-V material-based PV cells with a PCE of  $\approx 43.5\%$ .<sup>[26]</sup>

### 3. Development of PV-EC Technology for Solar Hydrogen Generation

The PV modules and electrolyzers are connected in series through wires, referred to as “traditional PV-EC” (Figure 3a). The other integrated configuration is called “integrated PV-EC,” which dramatically shortens the distance between the PV modules and the electrolyzers by coating the conducting layers and electrocatalyst layers contacting the electrolyte (Figure 3b). The integrated configuration allows limiting electrical and thermal losses (DC-DC converter, ohmic (cables and conductors), thermalization, and low energy photon absorption losses) inherent to traditional PV-EC.<sup>[5a]</sup> In addition, removing light absorbers from the electrolyte avoids the possibility of photoabsorber being corroded by the electrolyte. Stability against corrosion of the photoabsorbers in the aqueous media is of little concern. Moreover, the incident light enters the solar cell directly and is not attenuated by the surrounding electrolyte medium or by evolving gas bubbles.<sup>[27]</sup> In the following section, we will review the development history of these two distinct types of PV-EC technologies.

#### 3.1. Traditional PV-EC

The first PV-EC demonstration was conducted at the Jet Propulsion Laboratory in 1977.<sup>[28]</sup> A solar array of 175 W at 35 V from the Mariner 4 spacecraft was connected to a commercial electrolytic hydrogen generator. Two main components, PV modules and electrolyzers, are both superior pre-existing infrastructures, so it is not difficult to realize a large-scale system for PV-EC devices. Solar hydrogen projects in PV-EC were established in many places at the end of the 1990s (California, Germany, and Saudi Arabia).<sup>[29]</sup> However, this renewable method of hydrogen production suffered from low efficiency (2–6%), which increased project costs. With the use of both techniques, the performance of PV-EC devices has made progress in the past decades. This section will illustrate these respective PV-EC studies based on different PV materials.

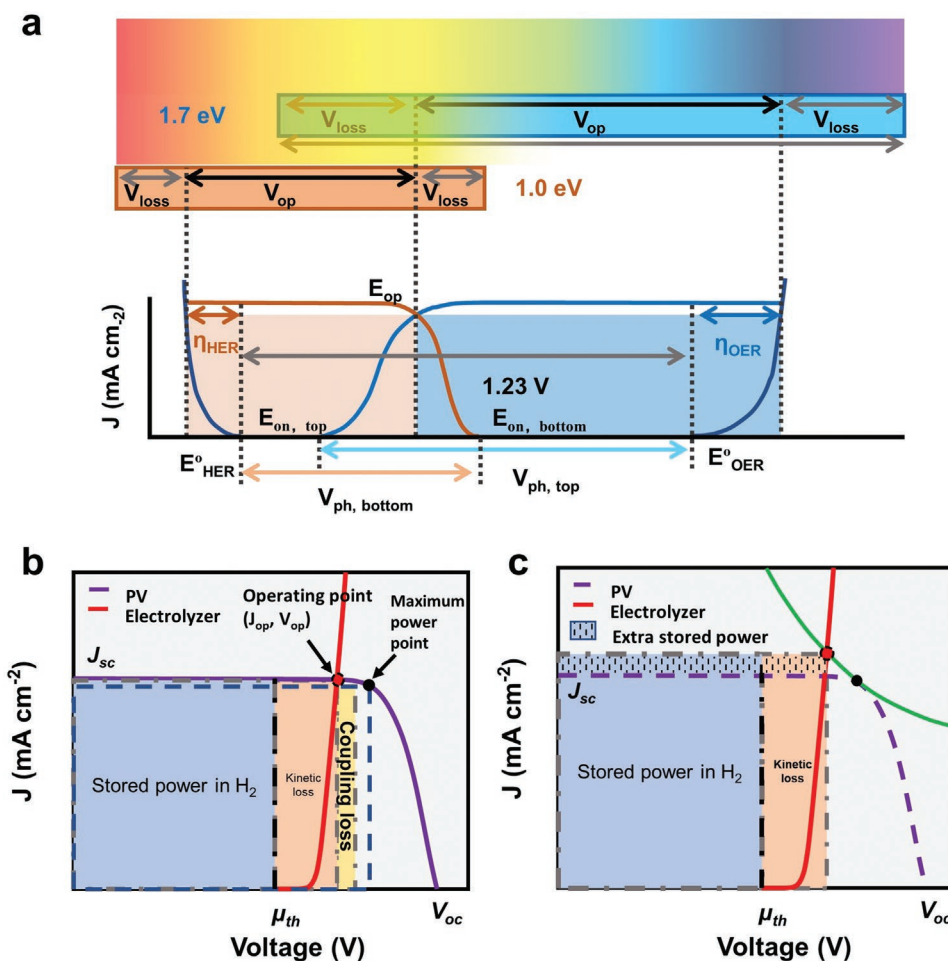


**Figure 4.** a) Schematic of bandgaps and  $J$ - $V$  curves for an idealized two-absorber tandem PEC cell, photoanode (blue, top absorber), and photo-cathode (orange, bottom absorber). Reproduced with permission.<sup>[11]</sup> Copyright 2017, Elsevier. The generalized current density–voltage ( $J$ - $V$ ) diagram of b) a directly coupled PV-EC device. Reproduced with permission.<sup>[24]</sup> Copyright 2013, National Academy of Sciences. c) The existence of a converter (PV-Conv-EC) graphically identifies the power flows relative to total incident solar irradiation. Reproduced with permission.<sup>[25]</sup> Copyright 2017, American Chemical Society.

### 3.1.1. Silicon (Si)-Based Systems

In the early stage, a large amount of auxiliary equipment was needed to ensure stable operation in a realistic outdoor environment. PV modules are connected to a charge controller, storage batteries, and DC–DC converter to match an electrolyzer operating at the MPP. However, the additional resistance imposed by the converters and batteries in these systems reduced the efficiency dramatically. In 2008, the simplification of the PV-EC was proposed by Gibson and Kelly.<sup>[29]</sup> The PV module was connected directly to the proton exchange membrane (PEM)-EC system. By designing the solar module to give maximum power at a voltage matching the fixed voltage required to operate the electrolyzer, they realized an STH efficiency of 12.4% based on the Si-based PV modules. A series of related works were demonstrated by the same group.<sup>[30]</sup> They constructed PV-EC for high-pressure (6500 psi, 44.8 MPa) hydrogen production using this direct coupling method, which achieved an STH efficiency as high as 9.3% and could supply  $\approx 0.5$  kg of hydrogen per day.<sup>[30a]</sup> The impact of a cloudy condition on the direct coupling

PV-EC was discussed,<sup>[30b]</sup> and a model was proposed for predicting the efficiency of Si-based PV modules and a PEM-electrolyzer system according to the parameters (such as the voltage, current, power, pressure, and temperature).<sup>[30c]</sup>

Since 2010, significant efforts have been made to replace noble-metal electrocatalysts with less expensive elements. With models based on steady-state equivalent circuits, Nocerab and co-workers believed that through a suitable design, the STH efficiency of PV-EC devices could reach 16% using commercial Si solar cells and earth-abundant components.<sup>[24]</sup> **Figure 5a** represents the modeling results with crystalline silicon (c-Si) solar cells and nonprecious electrocatalysts of NiMoZn (as the cathode) and Ni-Bi (as the anode).<sup>[31]</sup> The  $\eta_{STH}$  was estimated as 10% for the 4-cell in-series module of the c-Si solar cells. In 2016, with the high performance of Si heterojunction solar cells, an STH efficiency of 14.2% was obtained by combining three interconnected solar cells with microstructure Ni electrocatalysts.<sup>[19b]</sup> Recently, Chen et al. achieved the highest  $\eta_{STH}$  (16.9%) of Si-based PV-EC using a crystalline Si solar panel connected to catalysts (Co and Fe-codoped  $WO_{2.72}$  for OER and

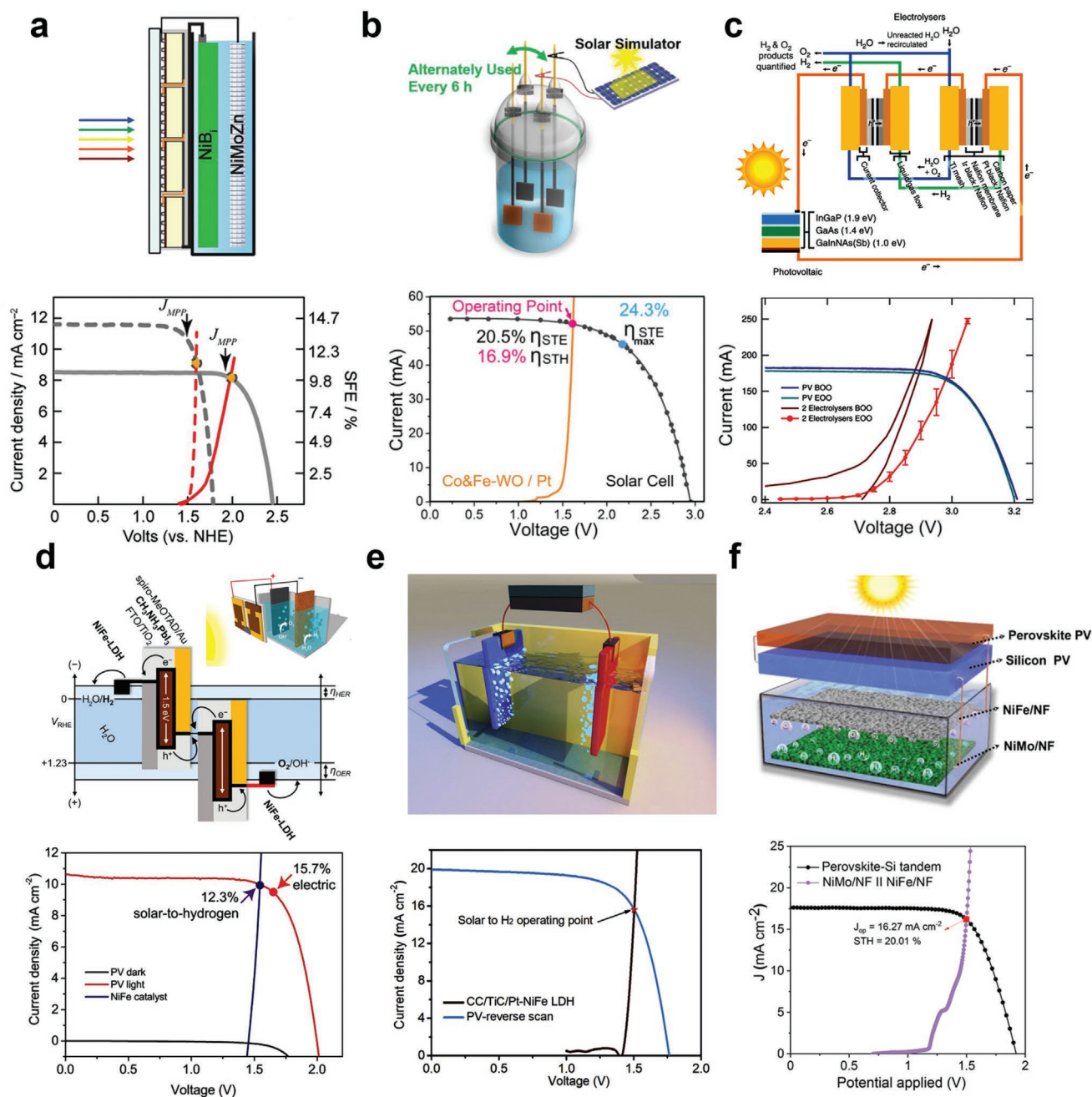


**Figure 5.** a) Four single-junction c-Si solar cells-NiBi/NiMoZn in 0.5 m  $\text{KBi}/0.5 \text{ m } \text{K}_2\text{SO}_4$ , pH 9.2. Reproduced with permission.<sup>[31]</sup> Copyright 2014, National Academy of Sciences. b) Si panel-Co&Fe-WO/Pt electrodes in a two-electrode configuration under 0.87-fold suns. Reproduced with permission.<sup>[32]</sup> Copyright 2019, John Wiley and Sons. c) One InGaP/GaAs/GaInNAsSb 3j solar cell-two series-connected PEM electrolyzers under 42 suns. Reproduced with permission.<sup>[5c]</sup> Copyright 2016, Springer Nature. d) Two series-connected PSCs- NiFe LDH/Ni foam in 1 m NaOH. Reproduced with permission.<sup>[19a]</sup> Copyright 2014, American Association for the Advancement of Science. e) A perovskite/Si tandem cell-NiFe LDH/Pt in 1 m KOH. Reproduced with permission.<sup>[18c]</sup> Copyright 2019, Elsevier. f) Perovskite-Si tandem cell integrated with NiFe/NF||NiMo/NF electrodes in 1 m KOH. Reproduced with permission.<sup>[35]</sup> Copyright 2021, John Wiley and Sons.

Pt on Ni foam for HER) immersed in 1 m KOH (Figure 5b).<sup>[32]</sup> Replacing OER and HER catalysts with  $\text{Co}_{0.4}\text{Fe}_{0.6}\text{MoO}$  and  $\text{CoMoO}$ , respectively, a PV-EC was demonstrated with a  $\eta_{\text{STH}}$  of 15.1% and no performance degradation over 160 h by the same group.<sup>[33]</sup>

### 3.1.2. III-V-Based Systems

III-V-based solar cells have been used to obtain higher STH efficiency, which offers much higher PCE than traditional Si-based systems. The record efficiency attained by a III-V-based

multijunction solar cell is 47.1%, whereas Si-based cells plateau at  $\approx 30\%$ .<sup>[34]</sup> Moreover, III–V materials allow the tailoring of bandgap and lattice parameters to access ideal energies while maximizing the crystalline quality. III–V materials can also be used under concentrated solar irradiation, increasing the current density of solar cells dramatically.

Research groups in Japan have systematically investigated III–V-based PV-EC from lab scale to sub-kilowatt scale.<sup>[36]</sup> In 2013, Fujii et al. demonstrated an STH efficiency of 13% under concentrated light from a solar simulator (8.2 suns) wiring the GaInP/InGaAs/Ge 3-tandem cell directly with a PEM electrolyzer.<sup>[36a]</sup> A wired combination of two series-connected GaInP/GaInAs/Ge cells and three series-connected electrolyzers was adopted to reduce the operating voltage mismatching, showing a higher STH efficiency of 15.3% under a 10-sun-equivalent solar simulator.<sup>[37]</sup> In 2015, Sugiyama and his co-workers conducted a field test combining a concentrator III–V-based PV module and a PEM electrolyzer, leading to an STH efficiency of 17.1%.<sup>[36b]</sup> With a higher-efficiency InGaP/GaAs/Ge three-junction cell ( $\approx 31\%$ ) and optimized number of elements in series (three PV and five EC cells), the system performance improved to 24.4% under 23 suns.<sup>[36c]</sup> This high STH efficiency occurs when the voltage between solar cells and electrolyzers matches. However, maintaining this condition is difficult, especially under fluctuating solar irradiance. Thus, in 2018, Ota et al. introduced a digitally controlled DC–DC converter into an expanded concentrator PV-EC, achieving a stable one-day STH efficiency of  $\approx 17\%$  on a sunny day.<sup>[36d,e]</sup> Performance ( $\approx 15\%$ ) was maintained even on a cloudy day.

Besides, Bonke and co-workers combined a GaInP/GaAs/Ge multijunction PV cell with Ni foam electrodes in 1 M NaOH.<sup>[38]</sup> An STH efficiency of 22.4% under 10 suns was obtained by adjusting the voltage match between the solar cells and electrolyzers. This high efficiency can be maintained over 24 h in such conditions. Follow-on work had the highest STH efficiency (over 30%) using one InGaP/GaAs/GaInNAsSb 3j solar cell and two PEM electrolyzers in series under simulated, concentrated solar light (Figure 5c).<sup>[5c]</sup> This system operated continuously for 48 h without interruption. Hsu and co-workers constructed a seawater-splitting device based on a single commercial III–V 3j photovoltaic cell.<sup>[39]</sup> The earth-abundant MHCM-z-BCC catalyst used in this device solved the evolution of undesirable chlorine on the anode. The catalyst assisted the seawater-splitting device in achieving high durability and specific selectivity toward OER in seawater with near 100% Faradaic efficiency with an STH efficiency of 17.9%.<sup>[39]</sup> Khan et al. constructed a concentrator PV-EC setup with an STH efficiency of 28% at 41 suns (without Fresnel lenses), which was the highest reported efficiency using an alkaline system to date.<sup>[40]</sup>

### 3.1.3. Perovskite-Based Systems

Luo and co-workers in 2014 first reported a PV-EC device with perovskite solar cells (PSCs),<sup>[19a]</sup> which is the first demonstration of PV-EC based on the PSCs. As shown in Figure 5d, two PSCs ( $\text{CH}_3\text{NH}_3\text{PbI}_3$ ) were placed side by side and connected with wires to immersed catalyst electrodes, where low-cost bifunctional earth-abundant NiFe-LDH was loaded on Ni foam.

This device gives an operating current of  $10.0 \text{ mA cm}^{-2}$  in alkaline electrolyte, corresponding to an STH efficiency of 12.3%. As solar cell prices were generally high at that time, the emergence of PSCs gave hope for constructing low-cost PV-EC and stimulated the rapid development of perovskite-based systems. However, the inherent instability of PSCs was a significant drawback of perovskite-based PV-EC, resulting in photocurrent degradation over hours. Improving stability and STH efficiency of perovskite-based PV-EC have become the development focus. The stability scale of perovskite-based PV-EC is significantly improved from hours to days due to the advanced encapsulation technology and novel interface engineering for PSCs.<sup>[41]</sup> For example, A long-term stability system with all-inorganic PSC ( $\text{CsPb}_{0.9}\text{Sn}_{0.1}\text{IBr}_2$ )- $\text{Ni}_{0.5}\text{Co}_{0.5}\text{P}$  nanowire array electrocatalysts can operate under continuous illumination for 24 h, while the STH efficiency is 3.12%.<sup>[42]</sup> To further improve STH efficiency, a bipolar membrane-assisted PV-EC was demonstrated using PSCs where CoP-Ti foam and NiFe LDH-Ni foam electrodes were immersed in 0.5 M  $\text{H}_2\text{SO}_4$  and 1 M KOH for the HER and OER, respectively.<sup>[43]</sup> High STH efficiency of 12.7% was achieved, establishing a new benchmark for the perovskite water-splitting device. As band-tunable property, perovskite is an ideal material for constructing a tandem solar cell with Si, showing both high PCE and low cost. A monolithic perovskite/Si tandem solar cell was introduced for the first time in PV-EC devices by Luo et al.<sup>[18c]</sup> Figure 5e shows that this novel hybrid tandem cell with an open circuit potential ( $V_{oc}$ ) of 1.76 V can drive water splitting. With Pt-based catalysts as the cathode and NiFe LDH as the anode in 1 M KOH, this device has an STH efficiency of 18.7% and can maintain 18.0% after 2 h. Replacing the Pt cathode with a NiMo-based catalyst, Wang et al. proposed a wire-connected perovskite-Si tandem cell-based PV-EC, achieving a record  $\approx 20\%$  STH efficiency and lasting for 15 h (Figure 5f).<sup>[35]</sup> In the same year, another setup refreshed the record efficiency using a self-reconstructed NiCoFe-based hydroxide nanosheet OER catalyst and the reported state-of-the-art HER catalyst  $\text{NiMo}_4/\text{MnO}_{3-x}$  connected to the monolithic perovskite/Si tandem solar cell.<sup>[44]</sup> An unprecedented STH efficiency of 21.32% was achieved and represented the highest value obtained by low-cost materials.

### 3.1.4. Other Traditional PV-EC Systems

Thin-film copper indium gallium selenide (CIGS) was another PV material used in PV-EC devices early in the 2000s. The device combined two illuminated CIGS cells with a  $\text{RuO}_2/\text{Pt}$  catalyst and achieved an STH efficiency of 4.29%.<sup>[45]</sup> The first demonstration of a 10% STH efficiency based on the CIGS was reported in 2013.<sup>[46]</sup> Three series of interconnected CIGS cells were fabricated by laser ablation, effectively connecting thin-film solar cells. Two different configurations were constructed by encapsulating glass and polymers or placing the absorber outside the electrolyte. Both have excellent STH efficiency of  $\approx 10\%$ , calculated by the current at the operating point and the amount of hydrogen produced, respectively. In addition, organic photovoltaics (OPVs) can contribute to large-scale photovoltaic energy conversion due to inexpensive, high volume, and solution-based manufacturing. The first OPV-EC device was

demonstrated by Esiner et al. using a solution-processed 3j polymer solar cell with a  $V_{oc}$  of 2.33 V.<sup>[47]</sup> A basic example of STH efficiency was illustrated by connecting two Pt electrodes in 1 M KOH electrolyte with estimated STH efficiency of only 3.1%. Although OPVs were generally less efficient than conventional inorganic PVs, remarkable improvements in their PCE have been observed in recent years,<sup>[48]</sup> and the STH efficiencies of OPV-EC devices have also increased from 3.1% to 10%.<sup>[49]</sup>

A direct connection is the most common method for traditional PV-EC research, avoiding the losses produced by DC–DC converters. The efficiency and stability of devices depend on the performance of PV cells and electrolyzers. A proper series–parallel structure between the solar cells and electrolyzers should be carefully adjusted, ensuring the operating point is near the MPP of the solar cells (Figure 4b). However, high-performance devices (III–V solar cells or PEM electrolyzers) are often expensive, which is an unfavorable factor for large-scale hydrogen production.<sup>[34]</sup> The optical losses of concentrated devices are the major problem suppressing further development in III–V-based PV-EC devices. Therefore, developing inexpensive and efficient PV cells and electrocatalysts is a high priority in the PV-EC field. The perovskite/Si tandem solar cell is a high potential candidate for high-performance PV-EC (STH efficiency > 20%), which needs to solve instability for large-scale applications.

### 3.2. Integrated PV-EC

The integrated PV-EC configuration appeared early in 1984.<sup>[50]</sup> Murphy and Bockris constructed a “one-unit water-splitting device” through two n/p-GaAs junctions arranged in series and coated on the dark sides with electrocatalyst layers (Pt foil and Ti/RuO<sub>2</sub>). The electrolyte was separated with semiconductors (GaAs) by the electrocatalyst layers. Sunlight illuminated the front of the semiconductor directly. While the stability was not reported, such a device gives ≈8% conversion efficiency of STH in 5 M H<sub>2</sub>SO<sub>4</sub> under one sun illumination. Multiple junction PV devices typically operate at high voltages, which is beneficial for constructing integrated PV-EC systems. For example, Rocheleau et al. developed a reactor for the direct photoelectrolysis of water to hydrogen using 3j amorphous silicon (a-Si) solar cells.<sup>[51]</sup> Electrocatalyst layers are NiFe<sub>y</sub>O<sub>x</sub> and CoMo, which can stabilize in 1 M KOH for more than 7200 h. An STH efficiency of 7.8% has been achieved in outdoor tests at the one-sun condition for direct photoelectrolysis of water. Subsequently, Turner and his co-workers obtained comparable results ( $\eta_{STH} = 7.8\%$ ) on a 3j a-Si (Pt) device in 1 M KOH.<sup>[52]</sup>

#### 3.2.1. III–V-Based Systems

Due to their high photovoltaic performance, integrated PV-EC systems are usually based on III–V multiple-junction solar cells. According to the pioneering work on a Pt/p-GaInP<sub>2</sub>/GaAs multijunction PEC cell,<sup>[16a]</sup> Khaselev et al. developed an integrated PV-EC device that is the same tandem cell but adds an n-GaInP<sub>2</sub> on top of p-GaInP<sub>2</sub>, improving the STH efficiency to 16%.<sup>[52]</sup> Licht et al. demonstrated that the  $\eta_{STH}$  could reach

18.3% based on bipolar configured Al<sub>0.15</sub>Ga<sub>0.85</sub>As ( $E_g = 1.6$  eV) and Si ( $E_g = 1.1$  eV) semiconductors.<sup>[18a]</sup> Inspired by the lab-scale experiment (an illuminated area of 0.22 cm<sup>2</sup>) of Licht et al., researchers at Fraunhofer Institute for Sol. Energy Systems (ISE) proposed a scale-up (8\*90.6 cm<sup>2</sup>) of the integrated hydrogen production system (HyCon module). They aim to achieve a conversion efficiency of >20% (based on the higher heating value of hydrogen) in an outdoor environment.<sup>[53]</sup> The configuration is shown in **Figure 6a**. A HyCon module consists of several Fresnel lenses focusing sunlight on each separate HyCon cell, where a III–V multijunction solar cell and a PEM-EC cell (Pt cathode/Ir anode) are contained. The solar cell is mounted on a copper heat sink and is directly integrated into the electrolyzer. The front side of the solar cell is connected to the cathode side of the EC cell via a cable. There were two generations of HyCon modules over a decade of development. The first generation module, where six parallel-connected tandem solar cells are located under an array of six Fresnel lenses, was constructed in 2006.<sup>[53]</sup> Each solar cell has an area of 3.14 mm<sup>2</sup>, and the whole module receives sunlight from 96 cm<sup>2</sup>, resulting in a concentration factor of 500. By adjusting the *I*–*V* curve of solar and EC cells and optimizing the structure of the flow-field pattern, the results of an outdoor measurement showed an STH efficiency of 16.8% (equal to 14.0% based on a lower heating value of hydrogen).<sup>[54]</sup> In 2016, the second-generation device was developed with area expansion. The number of HyCon cells, the area of the solar cell, and the Fresnel lens are increased to 8, 0.36 cm<sup>2</sup>, and 90.8 cm<sup>2</sup>, respectively.<sup>[55]</sup> Although scaling up the module, similar performance has also been obtained. This kind of system shows stable operation during 2 months of real-life conditions. High STH efficiency of 19.8% (equal to 16.5% based on a lower heating value of hydrogen) for current densities of 0.8 A cm<sup>-2</sup> with a Faraday efficiency of 98.5% at 252 suns was achieved.<sup>[56]</sup> High current densities in electrochemical components, resulting in large overpotentials for the water-splitting reaction, are unfavorable in integrated PV-EC. However, from an economic perspective, high current densities are especially beneficial for expensive electrocatalysts in PEM electrolyzers due to significantly improved utilization efficiency.<sup>[57]</sup> Recently, another integrated configuration based on a III–V-based photoabsorber and IrRuO<sub>x</sub>/Pt-based electrocatalysts was developed by Haussener and co-workers.<sup>[5a]</sup> As shown in **Figure 6b**, the device employed conduction and forced convection to cool the photoabsorber, heat the catalytic sites, and enhance the electrolysis kinetics. Intelligent, active thermal management and mass-transport optimization allow the integrated device to increase the current densities (≈0.88 A cm<sup>-2</sup>) at a calculated STH efficiency near 15% at 474 suns (using a high-power solar simulator rather than an optical concentrator).<sup>[5a]</sup> A similar integrated III–V-based PV-EC device with an alkaline EC cell was proposed recently in **Figure 6c**.<sup>[5b]</sup> Unlike the previous work, this device uses Ni foil directly as both OER electrocatalyst and to protect the layer, eliminating the expensive current collector components, such as copper heat sink<sup>[56]</sup> or Ti flow plate.<sup>[5a]</sup> Except for the high STH efficiency (13% at 207 suns), this integrated device can maintain a stoichiometric H<sub>2</sub>/O<sub>2</sub> ratio for >100 h tests. Stability is expected over 9 years based on the dynamic, secondary ion mass spectrometry experiment of the Ni surface.<sup>[5b]</sup>



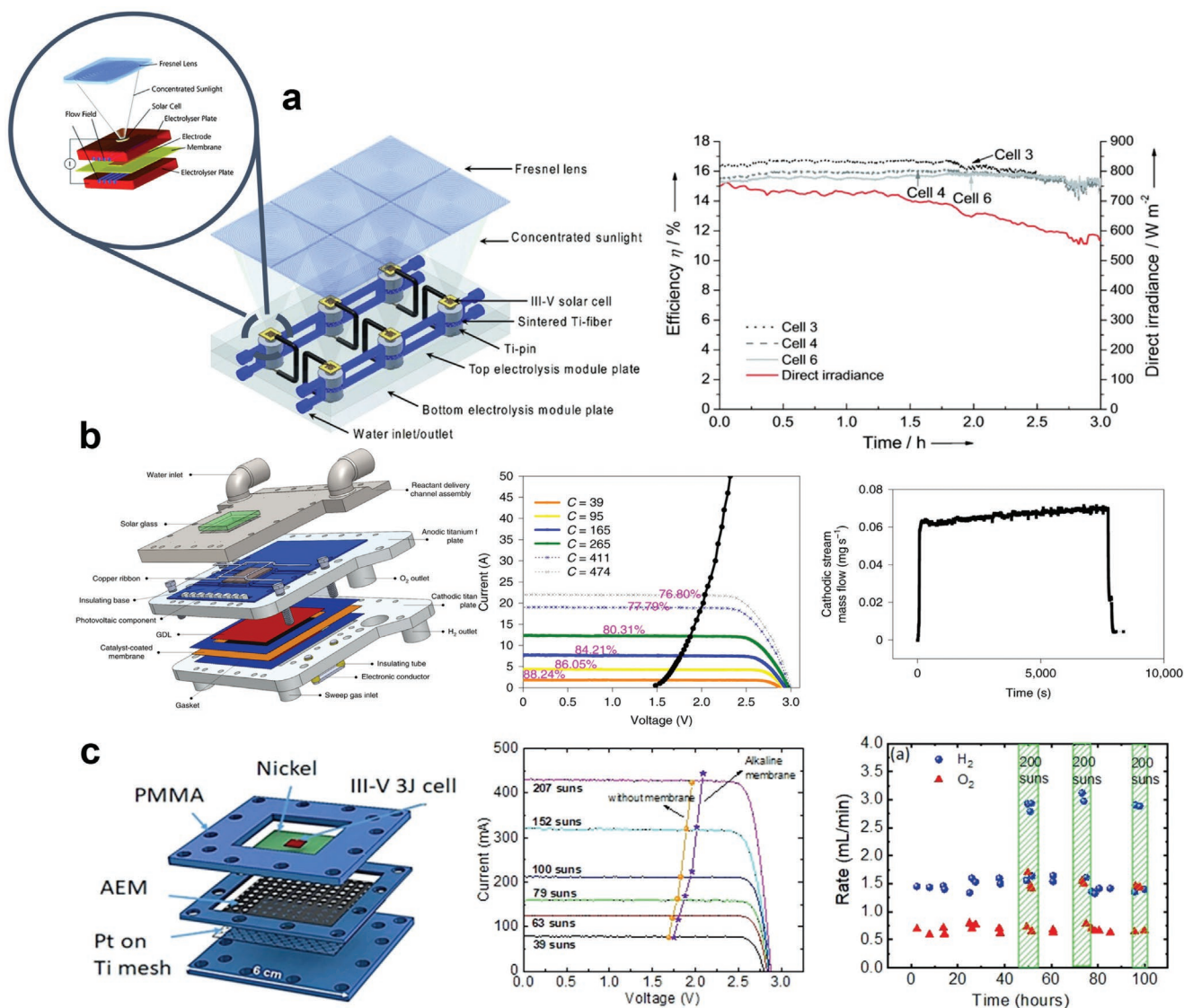


**Figure 6.** Demonstration of III-V material-based integrated PV-EC devices/systems. a) Integrated concentrated PV-EC system consisting of 6 HyCon modules, including a concentrator PV cell and a PEM electrolyzer. Reproduced with permission.<sup>[57]</sup> Copyright 2014, John Wiley and Sons. b) A 3j InGaP/InGaAs/Ge solar cell integrated with a PEM electrolyzer (IrRuO<sub>x</sub>/Pt) under 474 suns. Reproduced with permission.<sup>[5a]</sup> Copyright 2019, Springer Nature. c) A 3j GaInP/GaInAs/Ge PV cell-Ni/AEM/Pt in 5 M KOH under 207 suns. Reproduced with permission.<sup>[5b]</sup> Copyright 2020, John Wiley and Sons.

### 3.2.2. Si-Based Systems

Thin-film Si photovoltaic technology in integrated PV-EC has been investigated in the past 10 years. Most studies come from Forschungszentrum Jülich GmbH. In 2014, Ziegler et al. reported an integrated water-splitting device based on amorphous Si tandem solar cells with a  $V_{oc} = 1.8$  V. An STH efficiency of 5.5% was achieved with a Pt layer and a commercial RuO<sub>2</sub> counter electrode.<sup>[58]</sup> Later, Urbain et al. published an improved version of the device using an optimized ZnO:Al/Ag/Pt layer stack as the back contact, which protected the photovoltaic cell from the electrolyte and functioned as a catalytic layer for HER.<sup>[59]</sup> As a result, an STH efficiency of 6.8% combined with enhanced stability in diluted sulfuric acid (0.1 M H<sub>2</sub>SO<sub>4</sub>) was achieved. However, there were still challenges. For

example, the photovoltage was too low to operate the device at the MPP or in the photocurrent saturation plateau. The diluted electrolyte also led to additional ohmic loss. In 2016, Becker and his co-workers proposed a simple but valuable series circuit model to predict elaborately the PEC performance of an integrated device.<sup>[60]</sup> Guided by these theoretical results, Urbain et al. developed high-performance 3j solar cells consisting of amorphous (a-Si:H) and microcrystalline Si (μc-Si:H) for solar water splitting.<sup>[61]</sup> With the assistance of an Ag/Pt layer and RuO<sub>2</sub> as a counter electrode, the device showed excellent performance for an STH efficiency of 9.5%, which was the highest reported value for Si-based integrated water-splitting devices. Stability in strongly basic electrolytes was also a challenge. Pitting corrosion and delamination of the stacked layers led to an operation time of only a few minutes in 1 M KOH. However,

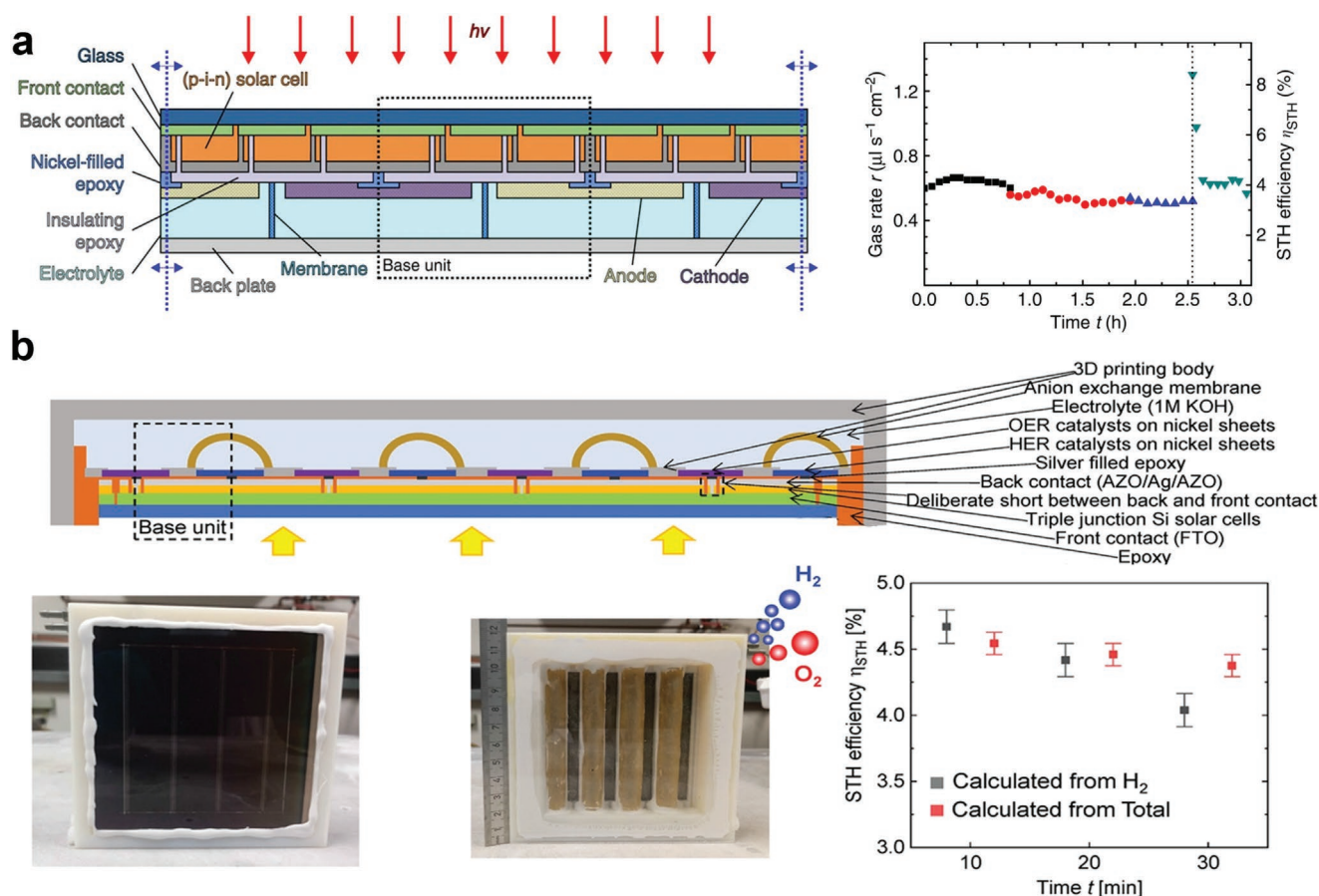


**Figure 7.** Large area ( $\approx 64 \text{ cm}^2$ ) demonstration of Si-based integrated PV-EC systems. a) The wireless device structure of a scalable, fully integrated photovoltaic water-splitting device and stability test. Reproduced with permission.<sup>[62]</sup> Copyright 2016, Springer Nature. b) Wireless PV-EC device based on a-Si:H/a-Si:H/ $\mu\text{c-Si:H}$  3j PV cell-bifunctional NiFeMo catalyst in 1 M KOH. Reproduced with permission.<sup>[63]</sup> Copyright 2020, John Wiley and Sons.

good stability for 4 h could be realized in a dilute basic electrolyte, although the ohmic resistance of the electrolyte and slower electrochemical kinetics limited the STH efficiency to 8.5%.<sup>[61]</sup>

For the technology to make a sizeable impact on the energy transition, Forschungszentrum Jülich GmbH has developed scale-up devices. **Figure 7a** presents their first reported scalable and wireless photovoltaic water-splitting device with an area of  $64 \text{ cm}^2$  in 2016.<sup>[62]</sup> Two spatially neighboring series-connected a-Si:H/ $\mu\text{c-Si:H}$  tandem cells were used as a base unit where the anodes and cathodes (nickel foam) were placed side-by-side on the backside of the PV element. The scale-up device was achieved by continuously repeating a base unit created by laser processing and showed a  $\eta_{\text{STH}}$  of 3.9% under a bias-free operation of 40 h in 1 M KOH.<sup>[62]</sup> In 2017, a stand-alone integrated PV-EC device with an active area of  $64 \text{ cm}^2$  was developed by the design of the front contact of multijunction thin-film Si solar cells.<sup>[64]</sup> During 80 min regular operation, the operating currents of 110 and 250 mA were established for the Ni/Ni and the Pt/IrO<sub>x</sub> catalysts, which correspond to STH efficiencies of 2.1% and 4.8% in an acid electrolyte and a base electrolyte, respectively. Replacing the Pt/IrO<sub>x</sub> with NiMo/NiFeO<sub>x</sub>, the device showed an STH efficiency of 5.1% and stability over 4 days.<sup>[8]</sup> Combining the 3j Si solar cell with the bifunctional NiFeMo catalyst, an upscale integrated PV-EC device was realized on a

3D-printed frame (**Figure 7b**).<sup>[63]</sup> The scaled-up device yields an STH efficiency of 4.67% but shows unsatisfactory stability of only 30 min.

Although integrated PV-EC is an attractive configuration in the solar water-splitting field, many challenges remain, especially in Si-based devices. In this configuration, the high STH efficiency ( $>5\%$ ) of Si-based systems has not been constructed for scale-up applications. Moreover, a stable structure of Si-based integrated PV-EC devices needs to be designed for extended operation, which is essential for practical application. Recently, Pehlivan et al. proposed an (Ag, Cu) (In, Ga)Se<sub>2</sub>-based integrated PV-EC from the lab scale ( $1.6 \text{ cm}^2$ ) to the  $100 \text{ cm}^2$ .<sup>[65]</sup> A maximum of 9.1% and 8.5% averaged STH efficiency for 100 h operation was obtained by combining four-cell interconnected PV modules with NiMoV-NiO electrolyzer. This device further demonstrated the advantage in thermal management and the significant room for improvement of the integrated PV-EC.

#### 4. Development of PEC Technology for Unassisted Solar Hydrogen Generation

The first publication of PEC hydrogen production devices can be traced back to 1972.<sup>[66]</sup> Fujishima and Honda demonstrated

the water electrolysis of hydrogen through an n-type TiO<sub>2</sub> semiconductor under light illumination. The spontaneous SLJ minimized the complexity of the device, promising the generation of clean fuels at a competitive cost. However, with a set of complex constraints, most semiconductors are suitable only for OER or HER, and an external bias is required for the overall water-splitting reaction. In practice, unassisted/unbiased PEC technology is desired, where the energy source is nothing but sunlight.<sup>[67]</sup> Therefore, photoanode–photocathode tandem cells, photoelectrode-PV cells, and buried-junction PEC cells are commonly constructed for unassisted water-splitting purposes.

#### 4.1. Photoanode–Photocathode Configuration

In 1975, the first unassisted photoanode–photocathode PEC cell was demonstrated with a p-GaP/n-TiO<sub>2</sub> tandem combination.<sup>[68]</sup> Despite that it showed only a 0.25% STH efficiency with the unstable cell, this result inspired the idea of water decomposition without bias. Due to the excellent stability and large  $E_g$ , many studies used TiO<sub>2</sub> or SrTiO<sub>3</sub> as the photoanodes to construct PEC cells with p-GaP, CuTiO<sub>x</sub>,<sup>[69]</sup> CaFe<sub>2</sub>O<sub>4</sub>,<sup>[70]</sup> or Si-based photocathodes.<sup>[71]</sup> The large  $E_g$  of photoanodes limits light absorption in the UV region, which accounts for only ≈4% of the solar spectrum, resulting in low STH efficiencies (<1%). Owing to their tunable optoelectronic properties, high light absorption coefficient, and exceptional charge-transport properties, III–V materials and their alloys are suitable for PEC cells.<sup>[34]</sup> Bockris and co-workers reported that a p-InN photocathode wired side-by-side with an n-GaAs photoanode achieved an STH efficiency of 8.2% and a lifetime of 10 h.<sup>[72]</sup> This demonstrated the best-performing photoanode–photocathode PEC cell presently. Despite high efficiencies, gallium or indium phosphides are not ideal for inexpensive large-scale production due to the scarcity of components with a single-crystalline requirement. To pursue economic PEC cells, interest in stable oxide materials was renewed in the 2000s.<sup>[73]</sup> Visible-light-responsive materials, such as Cu<sub>2</sub>O ( $E_g = 1.90–2.17$  eV), BiVO<sub>4</sub> ( $E_g = \approx 2.4$  eV), and Fe<sub>2</sub>O<sub>3</sub> ( $E_g = \approx 2.1$  eV), etc., have frequently been utilized due to their higher theoretical STH efficiencies and competitive cost.<sup>[14,74]</sup>

Cu<sub>2</sub>O is considered a promising and mature candidate for photocathodes for photoanode–photocathode tandem cell construction due to a theoretical maximum photocurrent of 14.5 mA cm<sup>-2</sup> and an STH efficiency of ≈18%.<sup>[75]</sup> However, the application of Cu<sub>2</sub>O has been inhibited by poor photostability in aqueous electrolytes. The modern era of Cu<sub>2</sub>O photocathodes began in 2011 by Parchino et al.<sup>[76]</sup> A p-Cu<sub>2</sub>O electrode was protected by the atomic layer deposition of Al-doped ZnO (AZO) and TiO<sub>2</sub> nanolayers and coated with electrodeposited platinum. This photoanode produced photocurrents as high as 76 mA cm<sup>-2</sup> at 0 V versus reversible hydrogen electrode (RHE) under one-sun illumination in 1 M Na<sub>2</sub>SO<sub>4</sub>. Stability was improved from seconds to days with protecting layers. The unassisted water-splitting cell with BiVO<sub>4</sub>/p-Cu<sub>2</sub>O tandem configuration was examined in 2014.<sup>[77]</sup> The intersection point of the  $J$ – $V$  curve gives an operating photocurrent density of 0.71 mA cm<sup>-2</sup>, representing 0.87% STH efficiency. An STH

efficiency of less than 0.5% with a two-electrode configuration was demonstrated after 100 s of operation. In 2018, using Ga<sub>2</sub>O<sub>3</sub> as an overlayer instead of AZO and constructing a nanowire structure, a Cu<sub>2</sub>O photoanode with a Ga<sub>2</sub>O<sub>3</sub> electrode showed a 0.5 V anodic shift (+1 V) in onset potential.<sup>[78]</sup> With NiMo as the HER catalyst and state-of-the-art BiVO<sub>4</sub> as the photoanode, ≈3% STH efficiency with ≈12 h stability was demonstrated in the electrolyte of 0.2 M KBi (Figure 8a). Further efficiency and stability improvements of Cu<sub>2</sub>O-based photoanode–photocathode tandem system were achieved in 2021.<sup>[79]</sup> A thin layer of covalent triazine frameworks containing a bithiophene moiety was introduced onto the surfaces of a Cu<sub>2</sub>O photocathode and a Mo-doped BiVO<sub>4</sub> photoanode via electropolymerization. The constructed unbiased PEC cell can achieve an STH efficiency of 3.70%. Even after continuous operation for 120 h, the STH efficiency remained at 3.24% (Figure 8b).

A similar  $E_g$  means a similar light absorption region, so Fe<sub>2</sub>O<sub>3</sub> is unsuitable as a photoanode for the Cu<sub>2</sub>O photocathode. Jang et al. reported that the onset potential of Fe<sub>2</sub>O<sub>3</sub> was realized around 0.45 V versus RHE using a facile regrowth strategy.<sup>[81]</sup> Finally, the efficiency of 0.91% and 10 h stability was achieved based on an earth-abundant hematite photoanode and amorphous Si photocathode. Due to the tunable light absorption range of the polymer-based semiconductors, the tandem cells of inorganic oxide- and organic polymer-based semiconductors provide a feasible solution for generating complementary light absorption. However, severe charge recombination and inefficient charge transfer hindered the STH efficiency of inorganic–organic hybrid PEC cells (<1.0%).<sup>[82]</sup> Recently, Ye and his co-workers utilized the charge-transfer mediators, the partially oxidized graphene (pGO) and SnO<sub>x</sub> for BiVO<sub>4</sub> photoanode, and CuO<sub>x</sub> and TiO<sub>x</sub> for organic polymer semiconductor (PIP), to facilitate charge separation and transfer in the photoelectrodes.<sup>[80]</sup> Figure 8c shows an unassisted PEC water-splitting system by coupling a Co<sub>4</sub>O<sub>4</sub>/pGO/BiVO<sub>4</sub>/SnO<sub>x</sub> photoanode and a Pt/TiO<sub>x</sub>/PIP/CuO<sub>x</sub> photocathode exhibited the highest STH efficiency of 4.3% for dual-photoelectrode PEC devices to date.

#### 4.2. PEC-PV Configuration

PV cells can provide a bias for semiconductors suitable only for OER or HER to construct unassisted overall water-splitting devices. The approach compromises device performance and complexity. A PEC-PV tandem device can be connected by wiring or preparing in a monolithic geometry. In the late 1990s, the monolithic configuration was proposed by Khaselev and Turner by combining p-GaInP with a GaAs p–n bottom cell via a low resistivity tunnel junction.<sup>[16a]</sup> The monolithic cell achieved an STH efficiency of 12.4% under 11 suns, a record for 20 years. Figure 9a shows a core–shell WO<sub>3</sub>/BiVO<sub>4</sub> nanorod photoanode assembled with a 2j GaAs/InGaAsP PV cell under reflected light from the photoanode, which gives an STH efficiency of 8.1% with no degradation for over 1 h.<sup>[83]</sup> Figure 9b presents a monolithic configuration with a GaInP<sub>2</sub>/GaAs/Ge 3j-based PEC cell covered by GaN nanostructures. The performance of  $\eta_{\text{STH}}$  (12.6%) with 57 h stability was achieved in a two-electrode measurement at zero bias.<sup>[5e]</sup>

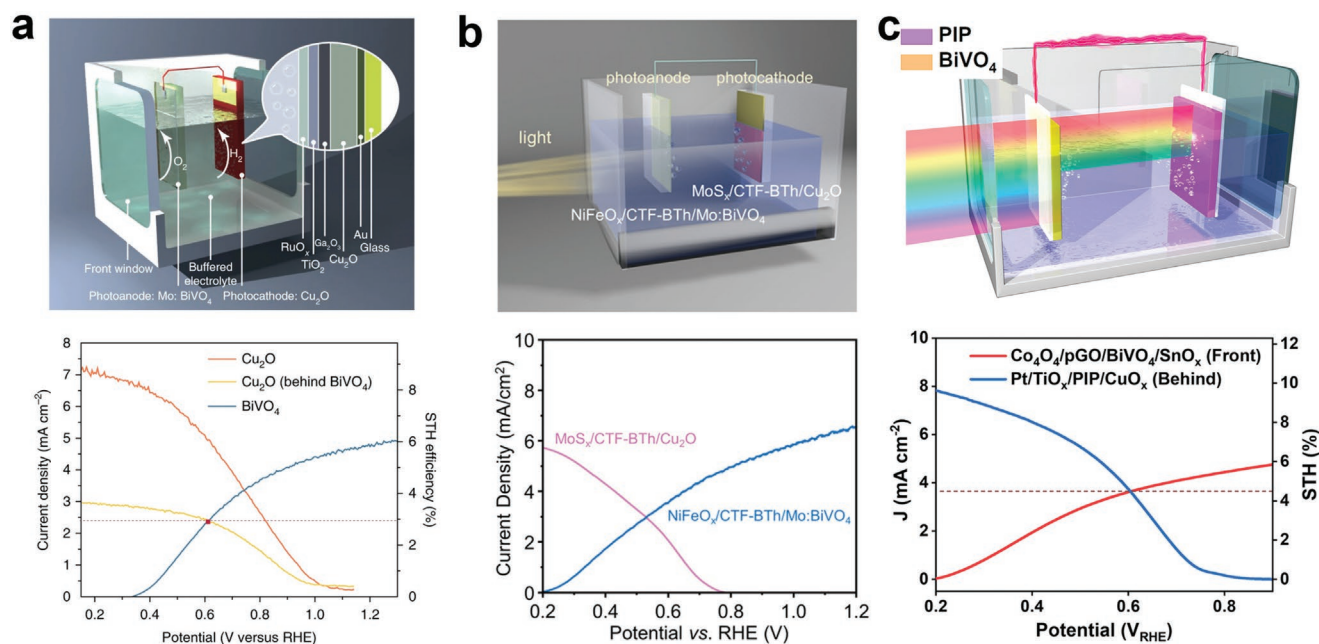


**Figure 8.** a)  $\text{RuO}_x/\text{TiO}_2/\text{Ga}_2\text{O}_3/\text{Cu}_2\text{O}$  photoanode and  $\text{Mo:BiVO}_4$  photocathode measured in 0.2 M potassium borate. Reproduced with permission.<sup>[78]</sup> Copyright 2018, Springer Nature. b)  $\text{MoS}_2/\text{CTF-BTh}/\text{Cu}_2\text{O}$  photoanode and  $\text{NiFeO}_x/\text{CTF-BTh}/\text{Mo:BiVO}_4$  photocathode measured in a 0.5 M borate buffer solution. Reproduced with permission.<sup>[79]</sup> Copyright 2021, John Wiley and Sons. c) PEC tandem cell with  $\text{Co}_3\text{O}_4/\text{pGO}/\text{BiVO}_4/\text{SnO}_x$  photoanode (front) wired to the  $\text{Pt}/\text{TiO}_x/\text{PIP}/\text{CuO}_x$  photocathode (behind). Reproduced with permission.<sup>[80]</sup> Copyright 2021, American Chemical Society.

Compared to III–V materials, some PEC-PV tandem cells use low-cost and earth-abundant materials, such as Si, dye-sensitized solar cells (DSSCs), PSCs, etc. Abdi and co-workers demonstrated a solar water-splitting device combining a gradient W-doped  $\text{BiVO}_4$  photoanode and a 2j a-Si solar cell. The stable photocurrent of  $4 \text{ mA cm}^{-2}$  corresponds to an STH efficiency of 4.9% under one-sun illumination (Figure 9c).<sup>[84]</sup> A novel strategy to enhance the efficiency of metal oxides by hetero-type dual photoelectrodes (Figure 9d) was proposed by Kim et al., where  $\text{BiVO}_4$  and  $\alpha\text{-Fe}_2\text{O}_3$  dual photoanodes were arranged in front of two c-Si solar cells in parallel.<sup>[85]</sup> The configuration extends light harvesting and increases the photocurrent in the photoanode. The unbiased water-splitting efficiency reached 7.7% and remained stable for over 8 h. Low-cost processes of solar cells that yield high photovoltaic output across the visible spectrum are required for large-scale hydrogen production. DSSCs and PSCs are potential candidates. A typical PEC-PV cell with a DSSC was demonstrated in 2012.<sup>[88]</sup> DSSCs with  $V_{oc} > 1.0 \text{ V}$  at one sun was designed by Yum et al., which allowed water splitting with one DSSC. Devices were assembled with nanostructured  $\text{WO}_3$  and  $\text{Fe}_2\text{O}_3$  photoanodes, and  $J_{op}$  was measured to give  $\eta_{STH}$  values of 3.10% and 1.17%, respectively.<sup>[88]</sup> The STH efficiencies of the photoelectrode-DSSC device were refreshed repeatedly by Shi and his co-workers.<sup>[89]</sup> High efficiency of 7.1% was demonstrated with a wireless configuration by introducing a Bragg reflector between (W, Mo)-doped  $\text{BiVO}_4/\text{WO}_3$  and DSSC.<sup>[89b]</sup> The Bragg reflector was transparent to the long-wavelength part of the incident solar spectrum ( $\lambda > 500 \text{ nm}$ ) for the rear DSSC and reflected the short-wavelength photons ( $\lambda < 500 \text{ nm}$ ) for total absorption of the front photoanode. The construction can significantly improve the operating photocurrent

and remain for over 10 h. PSCs are combined with various photoelectrodes, such as  $\text{TiO}_2$ ,<sup>[90]</sup>  $\text{BiVO}_4$ ,<sup>[86]</sup> or  $\text{Fe}_2\text{O}_3$ ,<sup>[91]</sup> with a similar configuration mentioned above. Gurudayal et al. combined a Sn-doped  $\text{Fe}_2\text{O}_3$  photoanode in a tandem design with a PSC ( $\text{CH}_3\text{NH}_3\text{PbI}_3$ ), showing an unassisted water-splitting process with an STH efficiency of 3.4%.<sup>[91]</sup> Figure 9e represents a high-performance PEC cell, which delivered a photocurrent density of  $5.01 \text{ mA cm}^{-2}$ , corresponding to an STH efficiency of 6.2%, by combining a nanocone  $\text{Mo:BiVO}_4/\text{Fe}(\text{Ni})\text{OOH}$  photoanode with a single PSC.<sup>[86]</sup> A stability test was performed over 10 h with only a 5.8% decrease. Wireless and dual photoelectrodes configurations were also applied in perovskite-based PEC-PV tandem cells. A tandem artificial-leaf-type cell produced stoichiometric hydrogen and oxygen with an average STH efficiency of 3.0% under one-sun illumination.<sup>[92]</sup> Two parallel  $\text{BiVO}_4/\text{FeOOH}/\text{NiOOH}$  dual photoanodes and a single sealed PSC can generate a photocurrent density of  $5.27 \text{ mA cm}^{-2}$  ( $\approx 6.5\%$  STH efficiency), with 3.8% decay after 10 h of consecutive light illumination.<sup>[93]</sup> Introducing oxygen vacancies, Kim et al. reduced both the photogenerated electron–hole recombination and  $E_g$  of barium stannate ( $\text{BaSnO}_3$  (BSO)).<sup>[94]</sup> The  $E_g$  decrease from 3.08 to 2.17 eV enhanced the absorption of visible light, exhibiting an increasing photocurrent density of  $7.32 \text{ mA cm}^{-2}$  at a potential of 1.23 V (vs RHE) with  $\text{FeOOH}/\text{NiOOH}$  catalyst. Combining with a PSC, an STH efficiency of 7.92% with 100 h stability was delivered. A polycrystalline Si (p-Si) photocathode operating in alkaline conditions was protected with a  $\text{TiO}_2$  passivation layer and edge-exposed  $\text{MoS}_2$  cocatalyst (Figure 9f).<sup>[87]</sup> The highest STH efficiency (6.6%) among the p-Si photocathodes was constructed by integrating an earth-abundant  $\text{Fe}_{60}(\text{NiCo})_{30}\text{Cr}_{10}$  anode and a perovskite/Si tandem photovoltaic cell.

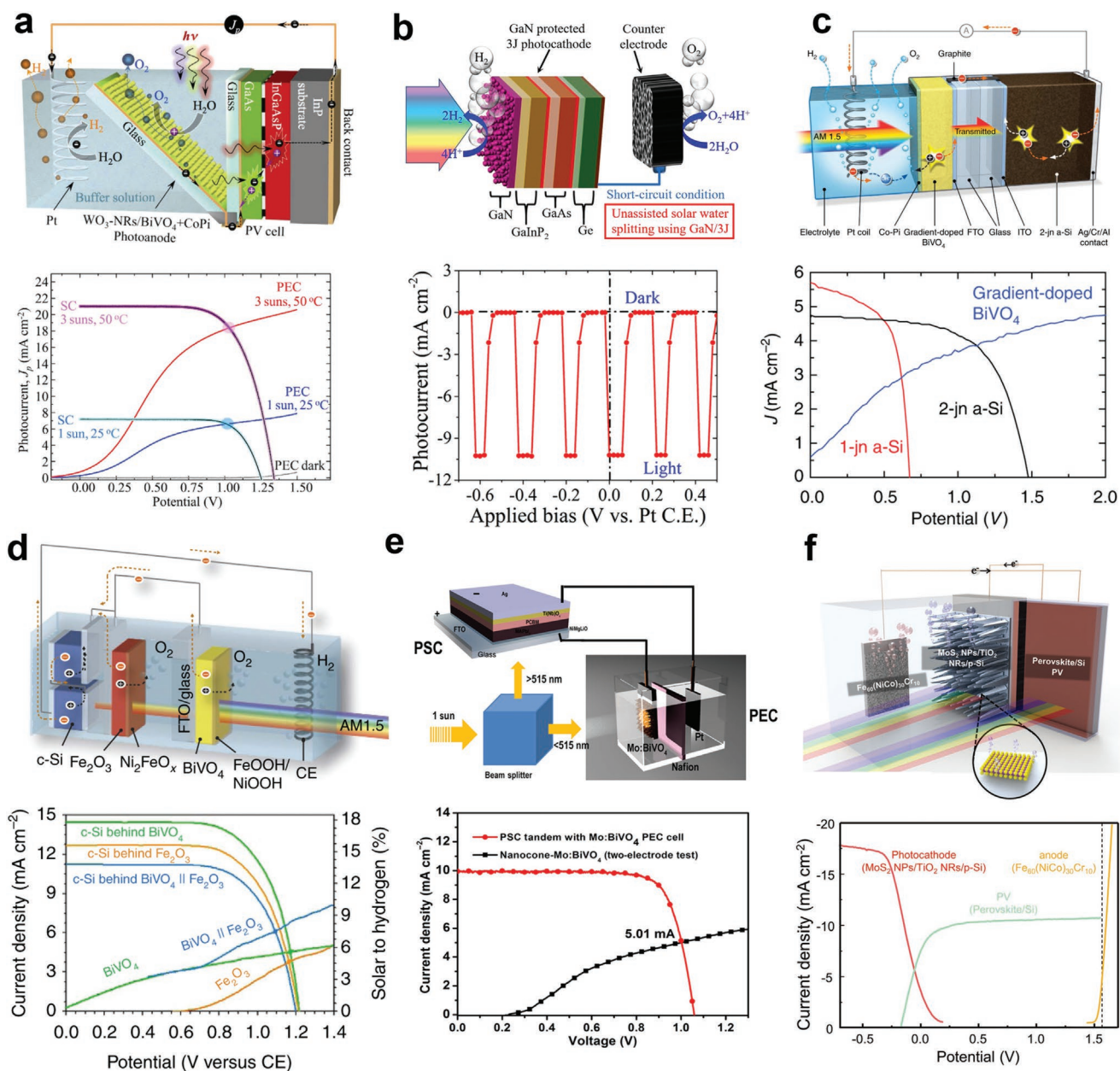


**Figure 9.** State-of-the-art free-bias photoelectrode–photovoltaic PEC cell for overall water splitting. a) A BiVO<sub>4</sub>/WO<sub>3</sub>-2j n-GaAs/InGaAsP tandem cell. Reproduced with permission.<sup>[83]</sup> Copyright 2021, Springer Nature. b) A p-GaN-3j GaInP<sub>2</sub>/GaAs/Ge tandem cell. Reproduced with permission.<sup>[56]</sup> Copyright 2019, American Chemical Society. c) A tandem configuration of gradient-doped BiVO<sub>4</sub> with an earth-abundant CoP water-oxidation catalyst and a double-junction a-Si solar cell. Reproduced with permission.<sup>[84]</sup> Copyright 2013, Springer Nature. d) A tandem cell equipped with a hetero-type dual photoanode (HDP) (BiVO<sub>4</sub>||a-Fe<sub>2</sub>O<sub>3</sub>) and a 2p c-Si solar cell. Reproduced with permission.<sup>[85]</sup> Copyright 2016, Springer Nature. e) A tandem configuration of nanocone-based Mo:BiVO<sub>4</sub>/PSC with a beam splitter application. Reproduced with permission.<sup>[86]</sup> Copyright 2016, American Association for the Advancement of Science. f) Noble metal-free tandem cell of the MoS<sub>2</sub> NPs/TiO<sub>2</sub> NRs/p-Si photocathode, perovskite/Si solar cell, and Fe<sub>60</sub>(NiCo)<sub>30</sub>Cr<sub>10</sub> anode. Reproduced with permission.<sup>[87]</sup> Copyright 2021, John Wiley and Sons.

### 4.3. Buried-Junction Configuration

Unlike SLJs, buried-junction PEC tandem cells are more attractive as the requirement for band edge positions of photoelectrodes which should be suitable for the potential of O<sub>2</sub>/H<sub>2</sub>O and H<sup>+</sup>/H<sub>2</sub> is unnecessary. Lin et al. reported the first buried-junction PEC cell with a wireless configuration by depositing Pt and RuO<sub>x</sub> on both sides of a 3j a-Si solar cell. A conversion

efficiency of ≈5% of STH at a steady state was achieved under simulated AM 1 (100 mW cm<sup>-1</sup>) solar radiation.<sup>[95]</sup> Replacing the novel metal catalysts (Pt and RuO<sub>x</sub>) with earth-abundant NiMoZn and Co-Bi, both wired and wireless devices were demonstrated by Reece and co-workers, as shown in **Figure 10a**.<sup>[7]</sup> The two devices maintained stable operation under one-sun illumination in KBi to observe  $\eta_{\text{STH}}$  of 4.7% and 2.5%, respectively. Although the 3j a-Si solar cells broke through the

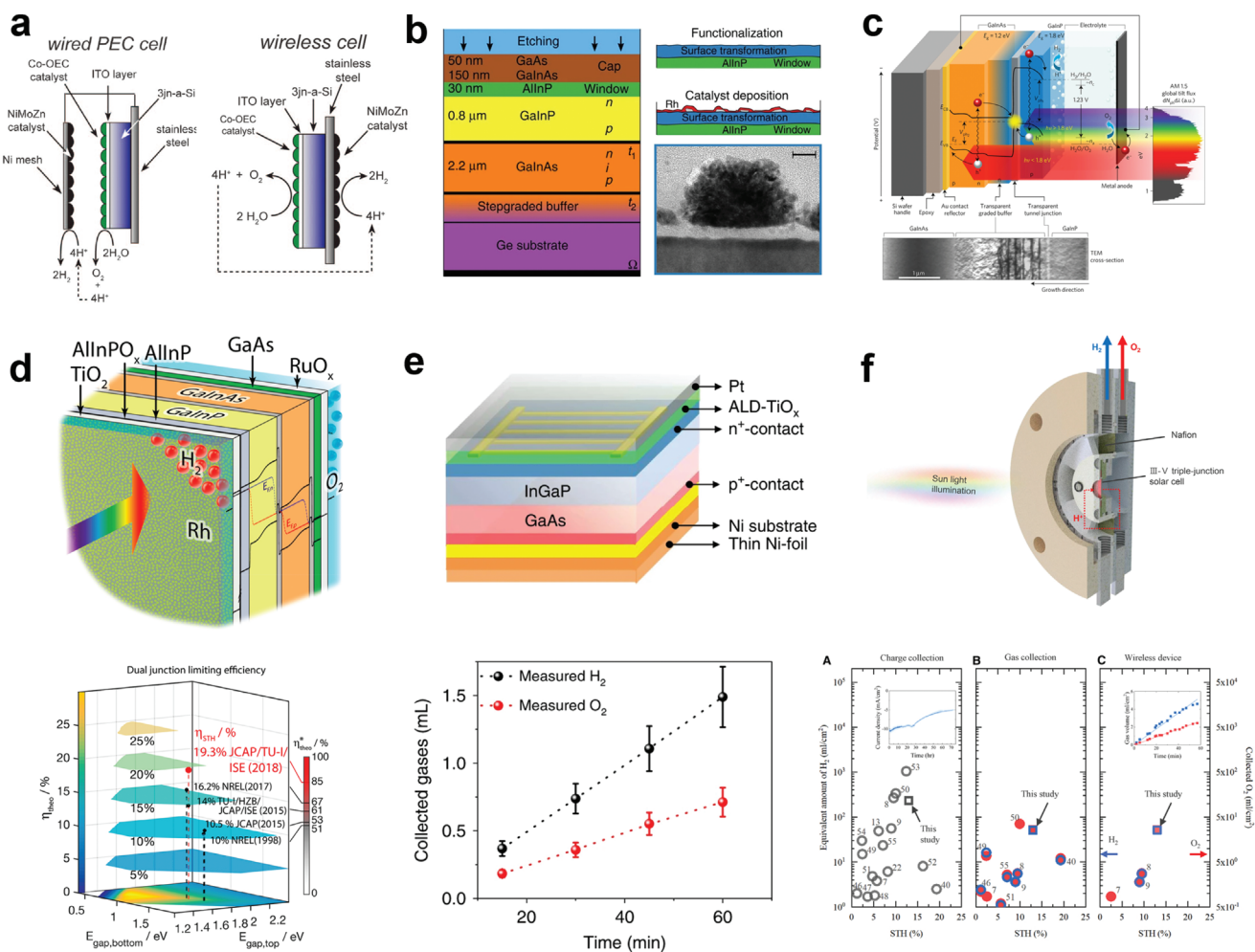


**Figure 10.** Typical unassisted buried-junction PEC cells for overall water splitting. a) A Co-Bi/3j a-Si/NiMoZn cell with wired and wireless configuration. Reproduced with permission.<sup>[7]</sup> Copyright 2011, American Association for the Advancement of Science. b) The tandem PEC with a GaInP n-p top cell and a GaInAs n-i-p bottom cell. Reproduced with permission.<sup>[97]</sup> Copyright 2015, Springer Nature. c) An IMM device architecture for maximizing light harvesting with GaInP ( $E_g = 1.8$  eV) and GaInAs ( $E_g = 1.2$  eV) junctions. Reproduced with permission.<sup>[23]</sup> Copyright 2017, Springer Nature. d) Buried-junction PEC configuration with Rh/TiO<sub>2</sub>/AllnPO<sub>x</sub>/AllnP-GaInP/GaInAs/GaAs/RuO<sub>x</sub>. Reproduced with permission.<sup>[98]</sup> Copyright 2018, American Chemical Society. e) Wireless device structure with the tandem cell of InGaP/GaAs and the O<sub>2</sub> and H<sub>2</sub> volumes measured for the device. Reproduced with permission.<sup>[15b]</sup> Copyright 2019, Springer Nature. f) Wireless solar water splitting using a III-V 3j solar cell (GaInP/GaAs/Ge) shows the highest hydrogen production value. Reproduced with permission.<sup>[15d]</sup> Copyright 2020, Elsevier.

constraints imposed by the minimum voltage requirements of water splitting, the low operating photocurrent cannot help PEC cells achieve high photocurrent densities. Thus, the STH efficiencies for most buried-junction PEC cells based on the 3j a-Si solar cells were always below 5%.<sup>[17,96]</sup>

III-V materials are a desirable candidate for buried junctions. However, III-V semiconductors corrode under HER and OER operating conditions<sup>[13,16a]</sup> and require protection in such applications. An amorphous TiO<sub>2</sub> layer was chosen to protect the tandem buried-junction GaAs/InGaP for PEC cell construction in conjunction with Ni-based electrocatalysts. The devices exhibited an STH efficiency of 10.5% when wired to a Ni-Mo-coated counter electrode in 1 M KOH.<sup>[99]</sup> In 2015, May et al. adopted a buried p-n junction tandem configuration with a GaInP n-p top cell and a GaInAs n-i-p bottom cell (Figure 10b). Coupling the tandem cell with Rh via in situ surface functionalization achieved a higher STH efficiency

of  $\approx 14\%$ , which extended the STH efficiency record for PEC cells after 20 years.<sup>[97]</sup> Figure 10c shows a buried-junction PEC tandem cell via 1.8/1.2 eV GaInP/GaInAs. An inverted-growth technique was utilized to avoid dislocations in the top higher-power junction, ensuring a higher overall efficiency (16.2%).<sup>[23]</sup> A p-n top-junction structure enhanced the photovoltage by 0.55 V over the traditional uniformly p-doped photocathodes (PEC-PV configuration). Subsequently, an improvement in 2018 achieved efficiency near the theoretical limits (85%) for the photoelectrode energy band gaps employed, which was also the maximum STH efficiency of 19.3% by a wired configuration characterization, the highest  $\eta_{STH}$  that a PEC device has achieved (Figure 10d).<sup>[98]</sup> Wireless configuration cells can be constructed with buried junction-type based on III-V materials. The monolithically integrated device consisted of a III-V 3j solar cell (InGaP/GaAs/Ge) with Pt (HER) and IrO<sub>2</sub> (OER) cocatalysts.<sup>[100]</sup> A  $\eta_{STH}$  of 11.2% was obtained by measuring the

rate of H<sub>2</sub> production under simulated one-sun illumination in 3 M KHCO<sub>3</sub>(aq) at pH 8.1. In 2019, Varadhan et al. reported an efficient PEC cell via an InGaP/GaAs double-buried junction (Figure 10e). Accessing the protective layer and electrocatalysts on both the front and back sides of the PEC device enabled by the unique epitaxial lift-off and transfer method gave a III–V-based unassisted-wireless device with a record  $\eta_{\text{STH}}$  of  $\approx 6.0\%$ .<sup>[15b]</sup> Very recently, the STH efficiency was improved to 13% over 12 h by both H<sub>2</sub> and O<sub>2</sub> products in a stoichiometric ratio (Figure 10f), which is the highest value reported from wireless PEC devices.<sup>[5d]</sup> In 2022, a versatile photoreactor system was designed with a MoS<sub>2</sub>/GaInP<sub>2</sub>/GaAs photocathode and an IrO<sub>x</sub> anode. An STH efficiency of 8.7% was obtained under real-world one-sun conditions, remaining an important step in the scale-up of PEC water splitting. An organic leaf was demonstrated by Esiner et al. based on a multijunction organic PV cell.<sup>[101]</sup> This buried-junction PEC device produced an average STH efficiency of 5.4% with low-overpotential RuO<sub>2</sub> catalysts

and 4.9% efficiency with earth-abundant NiMoZn-Co<sub>3</sub>O<sub>4</sub> catalysts and remained at 3.6% with a large area ( $\approx 1.7$  cm<sup>2</sup>).

In addition to the monolithic cell, the wired configuration gives more flexibility to construct different  $E_g$  combinations for buried-junction tandem cells.<sup>[4b,104]</sup> Luo et al. connected a low- $E_g$  ( $\approx 1.1$  eV) CIGS photocathode as a bottom absorber with a semi-transparent CH<sub>3</sub>NH<sub>3</sub>PbBr<sub>3</sub>-based solar cell, exhibiting an STH efficiency of 6.3% (Figure 11a).<sup>[102]</sup> Introducing ZnS between CIGS and CdS, Koo et al. improved the STH efficiency of the CIGS-PSC water-splitting tandem device to 8.61% and further increased to 9.53% with a stable operation of 6.5 h by a side-by-side configuration.<sup>[16b]</sup> Si with an  $E_g$  of 1.1 eV is another ideal material as a bottom absorber in tandem devices. Perovskite/Si dual-absorber tandem cells were demonstrated for stand-alone solar water splitting, showing an unprecedented 17.6% STH efficiency (Figure 11b).<sup>[103]</sup> In addition, an emerging low-cost material, Sb<sub>2</sub>Se<sub>3</sub>, with low  $E_g$  ( $\approx 1.18$  eV) exhibited massive potential for unbiased water-splitting devices.<sup>[104]</sup> Inserting a

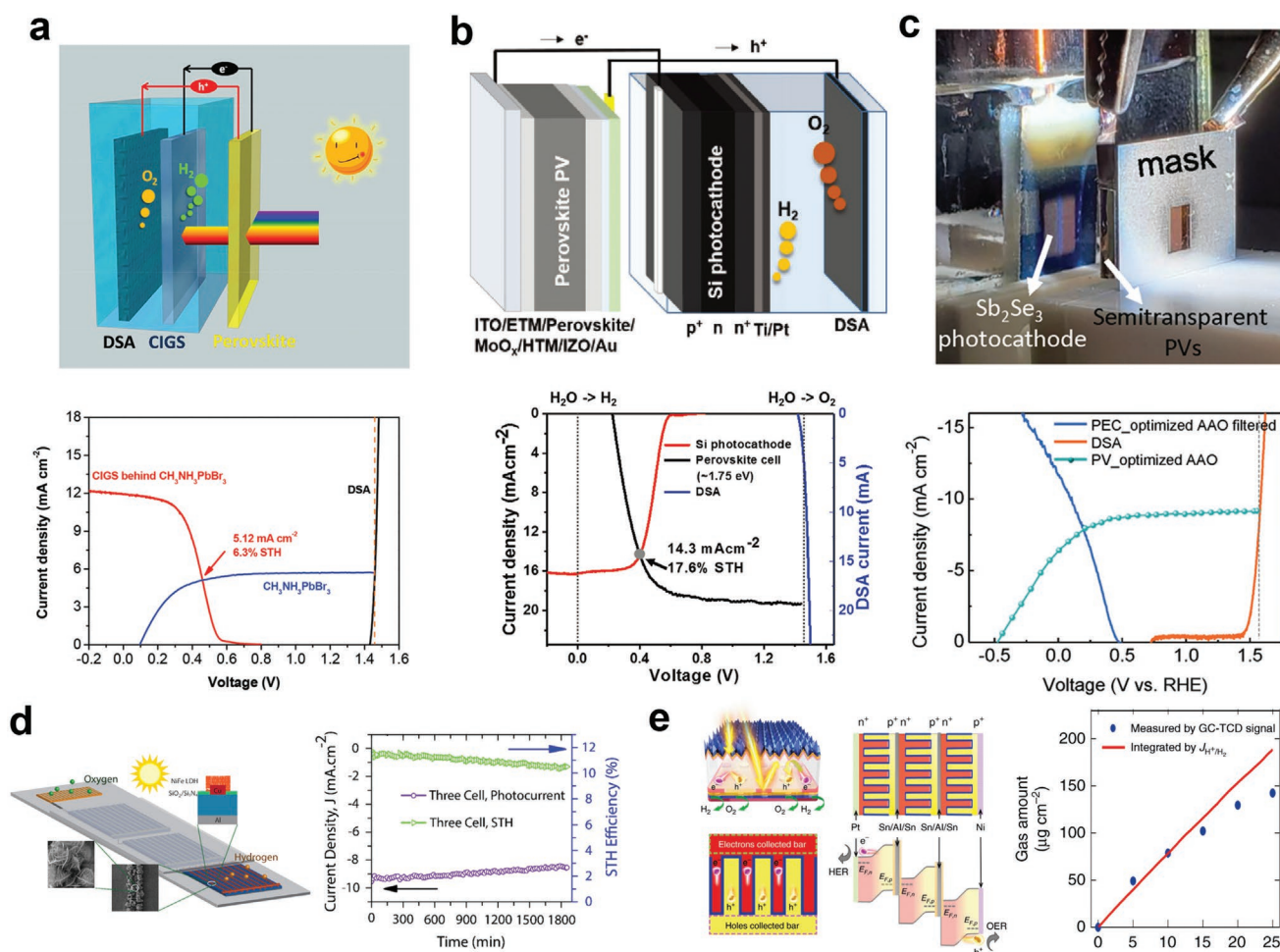


**Figure 11.** a) Perovskite and CIGS tandem water-splitting cell with a dimensionally stable anode (DSA) counter electrode. Reproduced with permission.<sup>[102]</sup> Copyright 2015, John Wiley and Sons. b) PSC wired to a Si photocathode in tandem and a DSA anode. Reproduced with permission.<sup>[103]</sup> Copyright 2020, John Wiley and Sons. c) The semitransparent PSCs, DSA, and Sb<sub>2</sub>Se<sub>3</sub> photocathodes behind the PSCs tandem device. Reproduced with permission.<sup>[104]</sup> Copyright 2020, John Wiley and Sons. d) Four series-connected c-Si solar cells integrated with bifunctional NiFe-LDH for overall water splitting. Reproduced with permission.<sup>[105]</sup> Copyright 2020, American Chemical Society. e) The schematic and band profile of the 3S-BBJ-PEC cell and the rate of H<sub>2</sub> production of the 3S-BBJ-PEC cell. Reproduced with permission.<sup>[5f]</sup> Copyright 2020, John Wiley and Sons.

SnO<sub>2</sub> layer on the TiO<sub>2</sub> layer increased the long-wavelength photon harvesting of Pt/TiO<sub>2</sub>/CdS/Sb<sub>2</sub>Se<sub>3</sub>/Au/fluorine-doped tin oxide, which is preferable as a bottom cell. A transparency-tunable parallelized nanopillar perovskite using an anodized aluminum oxide scaffold as the top cell constructed an optimum tandem device and achieved an STH efficiency of 10.2% (Figure 11c). The cell remains 80% after 10 h of continuous operation. Single-junction PV cells can drive overall water splitting through a series of interconnected configurations, as proposed by Jacobsson and co-workers.<sup>[46]</sup> Three CIGS PV cells were connected in series through the laser ablation method as a light absorber. Encapsulated with epoxy, the device presented an STH efficiency of ≈10% in 3 M H<sub>2</sub>SO<sub>4</sub>. Besides, single-junction PV cells can also drive overall water splitting through a series of interconnected configurations.<sup>[46]</sup> In Figure 11d, commercial single-junction Si solar cells were also demonstrated for unbiased water-splitting PEC cells. Only ≈2% of the total device area was covered by electrocatalysts, which minimized parasitic optical absorption of electrocatalysts, showing a high STH efficiency of 11.31%.<sup>[105]</sup> Using a back-buried junction design, Fu et al. showed >95% front-side light-harvesting PEC cells with a series interconnection configuration (Figure 11e). This nearly 100% light harvesting allowed the unassisted PEC cell to obtain an STH efficiency of 15.6% and a hydrogen generation rate of 240 μg cm<sup>-2</sup> h<sup>-1</sup>.<sup>[5f]</sup> The first self-powered over water-splitting PEC device using two monolithic PSC photoelectrodes was successfully constructed in 2020. With CoP- and FeNi(OH)<sub>x</sub>-based cocatalyst layers on the photocathode and photoanode, the integrated monolithic device achieved an STH efficiency of 8.54% and continuous stable operation of over 13 h. With a similar configuration, Rhee et al. improved the STH efficiency of a PSC-based integrated monolithic PEC device to 10.64% and could retain 60% of its performance after 20 h of operation.

From the above representative studies, unassisted water-splitting PEC cells with high STH efficiency and stability are accompanied by efficient charge separation and fast charge transfer, which are often difficult to achieve with simple SLJ alone. Thus, extra layers would be introduced to build homo- or hetero-junctions (typically p–n junctions, type-II hetero-junction, etc.). At the same time, the matching degree of the optical absorption of the two photoelectrodes determines the maximum theoretical efficiency of tandem cells. Therefore, in addition to layer structure engineering, suitable new types of inorganic semiconductors and organic polymer semiconductors/perovskites with tunable bandgap features have attracted more attention.

## 5. Techno-Economic Analysis

Progress in the basic research of efficient and durable solar water-splitting systems indicates consideration of practical applications through scale-up. According to the US Department of Energy (DOE) target, the levelized cost of hydrogen (LCOH) produced by water splitting using solar-driven electrochemical technologies could become competitive with that produced from fossil fuels if the price is reduced to about \$2.0–4.0 kg<sup>-1</sup> of H<sub>2</sub>.<sup>[22]</sup> Therefore, a techno-economic analysis of PV-EC hydrogen production systems comparing PEC (Type 1: traditional PV-EC, Type 2: integrated PV-EC, and Type 3: PEC

was performed. The cost predictions of solar hydrogen production systems have been performed in several comprehensive articles.<sup>[3c,22,106]</sup> However, the PEC used in most analyses is constructed on a back photoelectrode design. Although an “SLJ” exists between the metal electrocatalyst layer and the electrolyte, the light absorber is outside the electrolyte. The built-in electric field separating photogenerated charges are formed between the solid p–n junctions rather than the semiconductor and electrolyte. We prefer to define them as “integrated PV-EC.” In this study, we assessed a PEC based on an SLJ, formed once an inexpensive n- or p-semiconductor material contacts the electrolyte, simplifying the PEC and showing the advantages of the PEC structure. In addition, the three promising solar hydrogen systems are compared based on the state-of-the-art demonstrations. This analysis could thoroughly understand the impact that current technology and research breakthroughs could have on the financial viability of solar hydrogen production technologies and identify the gap between the current state of development and expectations for scale-up.

The LCOH in \$ per kg was applied in the analysis.<sup>[3c,22,106,107]</sup> Calculations took the net present value of the total cost of building and operating the hydrogen generating asset and were divided by the entire hydrogen generation over its lifetime, resulting in

$$\text{LCOH} = \frac{\sum_{t=0}^{t=n} \frac{I_t + M_t + F_t}{(1+r)^t}}{\sum_{t=0}^{t=n} \frac{H_t}{(1+r)^t}} \quad (4)$$

where  $I_t$  = the initial investment in year  $t$ ,  $M_t$  = the annual costs for maintenance and operation in year  $t$ ,  $F_t$  = the annual fuel costs in year  $t$  are usually zero in our solar hydrogen system, and  $H_t$  = hydrogen production (kg) in year  $t$ . The last two critical factors in the equation are  $r$  = the project discount rate and  $n$  = the lifetime of the system. A bottom-up evaluation method was applied to calculate the total system cost. All relevant components and cost parameters were performed, and total costs were calculated according to the size of the plant. **Table 1** lists the base-case design specification and financial parameters applied to the capital costs for three different systems to set the circumstances equal and realistic. The detailed techno-economic analyses are performed separately and compared with

**Table 1.** Operating and financial parameters used for all systems analyzed.

Parameter	Value
Hydrogen production rate	10 000 kg day <sup>-1</sup>
Plant lifetime	20 years
Hydrogen plant gate pressure	300 psi
Hypothetical plant site	Daggett, California
Construction period	1 year
Inflation rate	1.9%
Discount rate	12%
\$ basis year	2022



these solar hydrogen production technologies based on the analysis method and the baseline conditions mentioned.

### 5.1. Type 1: Traditional PV-EC

A direct connection is applied between PV and electrolyzer systems because the efficiency losses due to nonoptimal operation are similar to the efficiency losses incurred with a DC–DC converter that could provide optimal operation yet incur additional costs for the converter unit.<sup>[3c,29,106a,108]</sup> Table S1 and Figure S2 in the Supporting Information show the system-specific technical parameters and the distribution of the cost components (more detailed information in Table S2, Supporting Information). Since a traditional PV-EC consists of two parts, the PV modules and the electrolyzers, they are outlined separately.

Si is the standard material used in the industry for the current PV market due to its low cost, good efficiency, steadiness, and durability. A passivated emitter and rear cell initially developed at UNSW Sydney,<sup>[109]</sup> presently accounting for over 90% of commercial production with the highest efficiency of ≈25.0%.<sup>[110]</sup> Costs for this advanced Si photovoltaic module are taken from recent wholesale prices.<sup>[111]</sup> Hard-balance of system (BoS) costs, like wiring, panel mounting materials, and soft-BoS costs, are from recent utility-scale PV installations (Table S2, Supporting Information).<sup>[112]</sup> For the electrolyzer selection, although some novel techniques, such as solid oxide water electrolysis and anion exchange membrane (AEM) water electrolysis, are emerging, alkaline water electrolysis and PEM water electrolysis are the two primary methods for hydrogen production.<sup>[113]</sup> However, both slow current density altering and high minimum loads for operation (typically >20–50% of rated power) required by alkaline water electrolysis technology are causing significant challenges to the deployment for balancing intermittent renewable energy with a direct combination. In contrast, PEM electrolyzers rapidly respond to fluctuating input and have a wide load operation range tolerance (0–100%). Thus, the PEM electrolyzer is chosen as the main component, and average efficiency of 61% in its lifetime is desired.<sup>[106a,107b,113]</sup> According to the reasonable current production capacity of a PEM electrolyzer (≈10 MW year<sup>-1</sup>) reported by the DOE, a cost of \$458 kW<sup>-1</sup> is assumed, specifically \$270 kW<sup>-1</sup> for the stack and \$188 kW<sup>-1</sup> for the hard-BoS (power electronics/inverter excluded, about 51% of the original value).<sup>[114]</sup> Soft-BoS costs for a PEM electrolyzer, including engineering and design, installation, contingency, and expenses that arise from up-front permitting and overhead, are estimated to be 8%, 12%, 15%, and 15% of un-installed components cost.<sup>[115]</sup> The percentage of soft-BoS expenses will be used for the following two systems unless specifically emphasized.

Subsequently, the capital initial investment expenses can be obtained with the following mathematic calculations. To estimate the entire cost of the Si PV panels, the required area of panels with an STH of 15.25% was calculated for the given average sun irradiation (6.19 kWh m<sup>-2</sup> day<sup>-1</sup>) and capacity (10 000 kg<sub>H<sub>2</sub></sub> day<sup>-1</sup>) by Equation (5), resulting in ≈349 000 m<sup>2</sup>

$$\text{PV areas (A)} = \frac{n_{\text{H}_2} \cdot \Delta G_{\text{H}_2}}{P_{i,\text{average}} \cdot \eta_{\text{STH}}} \quad (5)$$

where  $n_{\text{H}_2}$  is the molar quantities of hydrogen production per day,  $\Delta G_{\text{H}_2}$  is the Gibbs free energy of hydrogen (at 25 °C  $\Delta G = 237 \text{ kJ mol}^{-1}$ ),  $P_{i,\text{average}}$  is the power density of average solar irradiance received on the PV modules per day, and  $\eta_{\text{STH}}$  is the system efficiency of STH. The required power of panels is calculated by Equation (6), resulting in ≈87 000 kW. The total PV cost was estimated by the price of its main components per Watt multiplied by the required power (Table S2, Supporting Information)

$$P_{\text{PV}} = P_{\text{AM1.5G}} \cdot A \cdot \eta_{\text{PV}} \quad (6)$$

where  $P_{\text{AM1.5G}}$  is the power density of solar irradiance of AM 1.5 G (100 mW cm<sup>-2</sup>) and  $A$  is the area of PV modules.  $\eta_{\text{PV}}$  is the PEC of the solar cell. Considering a direct connection of PV modules and PEM electrolyzers, the required power of the EC is designed for the maximum solar irradiance (925 W m<sup>-2</sup>) with Equation (7), resulting in ≈81 000 kW. Therefore, the total cost of the PEM electrolyzer system can be calculated similarly to that of the PV panels (Table S2, Supporting Information)

$$P_{\text{EC}} = P_{i,\text{max}} \cdot A \cdot \eta_{\text{PV}} \quad (7)$$

where  $P_{i,\text{max}}$  is the power density of maximum solar irradiance received on the PV modules over the year. The land cost was from data on the website of “Land of America,” which corresponds to \$1800 per acre.<sup>[116]</sup> Due to fixed panel arrays with a tilt angle of 35°, only shadowing from the south should be considered. Therefore, a separation of 2 m would result in shadowing only at angles below 26° at noon, which prevents the shadowing of the southward sun at its lowest angles.<sup>[117]</sup> Based on this consideration, the total land needed is two times the panel area, resulting in ≈172.5 acres, costing \$310 000.

Initial investment expenses, raw materials (water), utilities, labor, and other indirect costs compose maintenance and operational (M&O) costs of Type 1. In producing 10 000 kg day<sup>-1</sup> of H<sub>2</sub>, ≈91 m<sup>3</sup> of water is consumed daily, assuming 1% is lost due to evaporation.<sup>[106b]</sup> The price of demineralized water in the US is \$1.4 m<sup>-3</sup>,<sup>[106b]</sup> and thus, the yearly cost of water is about \$0.05 M. The electricity used in the plant powers the hard-BoS for PEM electrolyzers, such as heat exchanger cooling pumps, water pumps, and control systems. The yearly consumption is from the analysis performed by Directed Technologies Inc. (DTI) with the same capacity as our plant, resulting in 588 000 kWh.<sup>[117]</sup> Taking the price of electricity at \$0.069 kWh<sup>-1</sup> in the US, the total expenditure on electricity is \$0.04 M. Labor cost is location dependent. In this analysis, the labor cost assumption is based on an average salary of ≈\$30 h<sup>-1</sup> in the US in 2020.<sup>[118]</sup> Assuming automation, 10 people will ensure the proper operation of the plant. With the sun shining during the day, two 8 h shifts are considered per position.<sup>[107b]</sup> Therefore, 58 400 h per year is calculated, resulting in a total labor cost of \$1.75 M. Extra costs for maintenance and repair of PV and electrolyzer systems have been estimated. Solar panel operations and maintenance pricing are projected to fall to \$9.50 kW<sup>-1</sup> year<sup>-1</sup>. The maintenance and repair costs of the PEM electrolyzer are most commonly calculated as a fraction of uninstalled capital, and the value is assumed as 1.5% (Table S2, Supporting Information).<sup>[113]</sup> Finally, the PV modules were considered to last a lifetime of 20 years of the plant, but the lifetime of the electrolyzer stack is estimated to be 7 years.<sup>[3c,106a]</sup>

Accordingly, replacement components and labor costs (15% of uninstalled parts) for the stack should be considered every 7 years (Table S2, Supporting Information). Note that the same time interval and labor cost proportion of replacement is assumed in the following two systems.

## 5.2. Type 2: Integrated PV-EC

Integrated PV-EC has advantages in thermal management, which can be utilized by the structure of concentrated III–V solar cells and PEM electrolyzers.<sup>[5a]</sup> First, the heat from concentrated irradiance on solar cells can quickly transfer into the electrolyzers through the metal catalyst layer. The solar cell should be as cold as possible while the electrolyzer should be heated, which promotes the performance of both components. Meanwhile, the PEM electrolyzer can operate at a high current density, improving the utilization rate of precious metal catalysts (such as Pt and IrO<sub>x</sub>) and reducing cost. Unlike the traditional PV-EC, large-scale-integrated PV-EC is not available commercially, but Fraunhofer ISE has demonstrated a feasibility size of 8\*90.6 cm<sup>2</sup> under outdoor conditions.<sup>[84]</sup> Therefore, we proposed a large-scale-integrated PV-EC by repeating the basic units (HyCon module). High-concentration Fresnel lenses reduce costly solar cell materials, and the area ratio remains at 252 between the lenses and solar cells. A lattice-matched combination of three p–n junctions (3J) of GaInP, Ga(In)As, and Ge is used with a PCE of ≈33%.<sup>[119]</sup> A PEM electrolyzer was applied and contacted the GaInP/Ga(In)As/Ge solar cell. Finally, given that Fresnel lenses as light concentrators lead to optical losses of ≈25% in previous research, an adjusted STH efficiency of ≈15% is assumed.

Table S3 and Figure S3 in the Supporting Information list the technical parameters and a cost overview, respectively, and detailed information for every component cost is shown in Table S4 in the Supporting Information. A near-range predicted cost for a high-efficiency 3j GaInP/Ga(In)As/Ge solar cell was assumed to be \$80 W<sup>-1</sup>.<sup>[119]</sup> The system concentrates direct radiation onto the solar cell with little diffuse radiation. A dual-axis solar tracker ensures that the reactor receives direct irradiance throughout the day.<sup>[117]</sup> Due to the tracker, the average solar irradiance can reach 6.55 kWh m<sup>-2</sup> day<sup>-1</sup>, which leads to a receiver area (Fresnel lenses) of ≈330 000 m<sup>2</sup> (Equation (5)). With a concentrated factor of 252, the critical area of the GaInP/Ga(In)As/Ge solar cell is about 1310 m<sup>2</sup>, corresponding to ≈430 000 W (Equation (6)). The total cost of 3j GaInP/Ga(In)As/Ge solar cells is \$32.62 M. For the Fresnel lenses, both materials and size influence price. A size of 1010\*1010 mm for a single lens was adopted, and poly(methyl methacrylate) (PMMA) was chosen to enhance light transmission. The \$100 m<sup>-2</sup> cost is the recent wholesale price.<sup>[120]</sup> The heat sink is made from copper due to its high thermal conductivity. We assumed that the area of a heat sink is 25 times that of solar cells, and the thickness is ≈1 mm. The price of copper is roughly \$9.60 kg<sup>-1</sup>, resulting in \$2.82 M.<sup>[121]</sup> The wiring cost is neglected because 3j III–V solar cells are directly connected with the bipolar plate by the copper heat sink; only a few cables are used in the system. The electrolyzer is sized to accept the maximum instantaneous power output by the photovoltaics, assumed to be ≈650 W m<sup>-2</sup>. The

required power for EC (70 356 kW) was estimated by Equation (7). The principal components (bipolar plate, porous transport layer, membrane, and catalysts) and hard-BoS are identical to those of Type 1. The results are shown in Table S4 in the Supporting Information. BoS is considered in the analysis. The dual-axis solar tracker cost of \$0.16 W<sup>-1</sup> is assumed.<sup>[122]</sup> A weatherproof housing chassis protects the reactor outdoors, taking PMMA, and the cost is \$7.39 W<sup>-1</sup>.<sup>[3c]</sup> With a solar tracker, the land cost was calculated at 6.57 times that of Fresnel lenses.<sup>[117]</sup> Soft-BoS and M&O expenses for Type 2 are the same as those of Type 1 (Table S4, Supporting Information).

## 5.3. Type 3: PEC

A PEC with an SLJ is considered.<sup>[13]</sup> Unlike fully buried PV junction PEC devices, this configuration would be achieved by a photoelectrode composed of single inexpensive semiconductor material in the ideal cases, which is always considered one of the most potent ways to achieve solar hydrogen at a lower price.<sup>[11,12b]</sup> An efficient unbiased system cannot be constructed just by a single SLJ. Specifically, unassisted PEC water-splitting devices are tandem cells with photoanode–photocathode or photoelectrode-PV configuration. Although the highest theoretical STH efficiency of tandem PEC cells is ≈30%,<sup>[26,123]</sup> the practical efficiency is lower (usually <5%). Therefore, a photoelectrode-PV configuration was chosen with some assumptions. One assumption is that the STH efficiency of the large-scale PEC is based on lab-scale studies with no scale-up degradation. An STH efficiency of 6.2% was selected in this analysis, one of the highest efficiencies of photoelectrode-PV with a single inexpensive oxide semiconductor material. In the demonstration, BiVO<sub>4</sub> was chosen because of its low cost, high stability against photocorrosion, and narrow E<sub>g</sub> of 2.4 eV. Instead of a single PSC, two parallel-connected c-Si solar cells with the same area as BiVO<sub>4</sub> produce enough power to provide the same current density (5.01 mA cm<sup>-2</sup>), which was proven by Kim et al. The same earth-abundant cocatalysts (like FeOOH/NiOOH) are deposited on BiVO<sub>4</sub> to improve the charge carrier injection efficiency to the electrolyte.<sup>[85]</sup> Ni mesh is chosen in a 0.5 M KH<sub>2</sub>PO<sub>4</sub> buffer solution for the counter electrode. Finally, the Nafion membrane is used to avoid mixing the produced H<sub>2</sub> and O<sub>2</sub>. The membrane area is assumed to be 10% of the photoabsorber area. Although higher STH efficiency can be achieved by introducing III–V materials, the high price inhibits their development, especially in nonconcentrated systems.

The specific technical parameters and cost distribution of Type 3 are summarized in Table S5 and Figure S4, in the Supporting Information, respectively. More detailed cost information is provided in Table S6 in the Supporting Information. The PEC panel area is ≈86 000 m<sup>2</sup> (Equation (5)). The core component is the photoelectrode, composed of a glass substrate coated with a transparent conductivity oxide (TCO) layer, a metal oxide semiconductor, a Si solar cell, and cocatalysts. In this system, we estimate the cost of BiVO<sub>4</sub> with a bottom-up method. The primary raw reagents are summarized in Table S7 in the Supporting Information. The total quantities of BiVO<sub>4</sub> are calculated, resulting in ≈6700 kg<sup>[86]</sup> and a cost of \$4.51 M. TCO is used to collect the electronics from BiVO<sub>4</sub>, and the price was

assumed to be about  $\$11 \text{ m}^{-2}$ . Poly c-Si solar cells are selected with the same area of  $\text{BiVO}_4$ , costing  $\$0.11 \text{ W}^{-1}$ .<sup>[111]</sup> Earth-abundant cocatalysts and the counter electrode are chosen to reduce system cost. Their cost from the previous analysis is  $\$5$  and  $\$0.5 \text{ m}^{-2}$ , respectively. The ion exchange membrane costs  $\$1098 \text{ m}^{-2}$  and is 10% of the area of PEC panels.<sup>[114]</sup> Soft-BoS costs for PEC are the same as those for Type 2, except that the contingency is increased to 30%, a typical value in chemical engineering plants with novel technologies.<sup>[106b]</sup> One item differs from the last two systems in M&O expenses due to the gas compressor. More electricity will be needed in the PEC, totaling  $\$0.05 \text{ M year}^{-1}$ . For replacement costs, except for poly c-Si solar cells, PEC panels should be replaced every 7 years, and 15% of labor is included, like the last two systems.

#### 5.4. Sensitivity Analysis

Given the initial investment, M&O and replacement expenses, and the technical parameter assumptions, the LCOH for Type 1, Type 2, and Type 3 were  $\$6.70$ ,  $\$9.16$ , and  $\$14.60 \text{ kg}^{-1}$ , respectively. All LCOH values are far from the DOE's target ( $\$2.0 \text{ kg}^{-1}$ ). A sensitivity analysis based on consistent values ( $\pm 20\%$  of the base value for each parameter) is implemented to show the effects on costs. Soft-BoS costs are a proportion of the uninstalled capital expenses, which means they are directly dependent on the other expenses; therefore, they are not considered separately.

The sensitivity analyses for the three systems are shown in Figure 12. STH efficiency is the most sensitive parameter. For Type 1 (Figure 12a), the electrolyzer cost is the second most sensitive parameter. Therefore, to decrease the LCOH of Type 1, we should focus on developing electrolyzers at a reduced cost. Because of the high price components, such as III–V solar cells and Fresnel lenses, used in Type 2, the concentrated PV and electrolyzer costs have similar effects on the LCOH (as shown in Figure 12b). Cost reductions of these components are a priority to decrease the LCOH for Type 2. The lifetime influence for Type 1 and Type 2 is lower than other parameters. However, as shown in Figure 12c, lifetime is a sensitive parameter for Type 3. Increasing the STH efficiency and lifetime of PEC devices are the two most effective ways for LCOH reduction in Type 3. Photoactive materials are chosen as the low-price oxide semiconductor, so the cost of Nafion membranes is more sensitive to LCOH for Type 3.

#### 5.5. Potential Cost Reduction

The potential costs of the three systems and related technologies will be analyzed based on sensitivity analysis. The results are shown in Figure 13.

Type 1 approximates the present state of the traditional PV-EC as the techniques and economic parameters are currently available. To further reduce LCOH, higher STH efficiency is needed according to the sensitivity analysis. The highest efficiency of the c-Si solar cell is 26.7% with the n-type rear Interdigitated Back Contact technique (IBCC).<sup>[124]</sup> The PEM electrolyzer efficiency is expected to increase to 74%.<sup>[113]</sup> Moreover, a longer life will

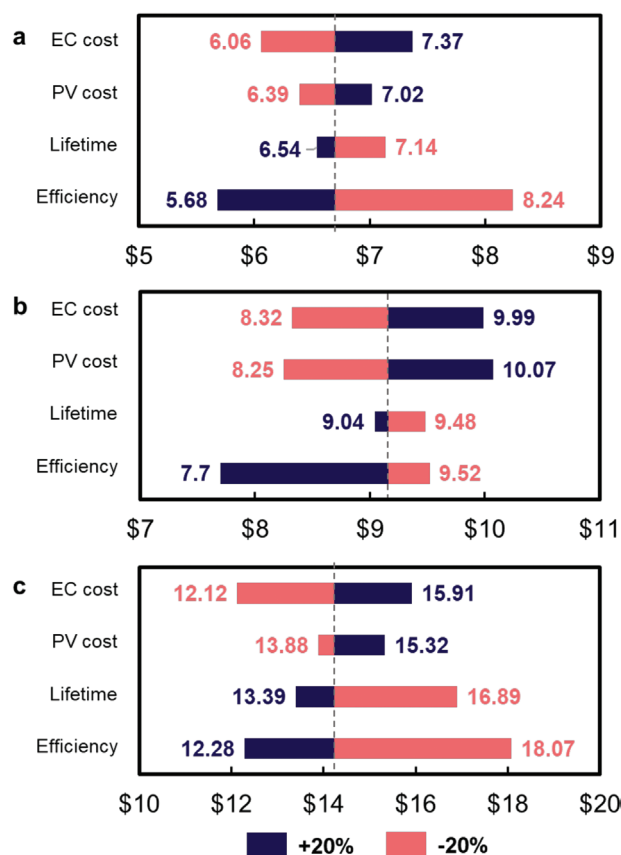


**Figure 12.** Sensitivity analysis based on STH efficiency, lifetime, and principal components costs for a) Type 1; b) Type 2; c) Type 3.

lead to lower replacement costs. In an ideal situation where the lifetime of the PEM electrolyzer stack is longer than 20 years, the replacement cost is expected to be zero, resulting in an LCOH of  $\$5.02 \text{ kg}^{-1}$ . The PV and electrolyzer costs are the main components influencing the LCOH of Type 1 (Figure 13a). For PV cost, the price of PV modules is crucial. Because the current price of solar cell modules is affected by COVID-19, the price is expected to reduce after the pandemic. A cost of  $\$0.2 \text{ W}^{-1}$  is anticipated for the IBCC/PEC solar cell module in the future.<sup>[125]</sup> The electrolyzer cost is projected to be reduced, especially with factory scale-up.  $\$79$  and  $\$114 \text{ kW}^{-1}$  are used for this analysis cost of PEM electrolyzer stacks and hard-BoS for  $1000 \text{ MW year}^{-1}$ .<sup>[114]</sup> Combining all optimistic assumptions, the final LCOH for Type 1 decreases to  $\$3.62 \text{ kg}^{-1}$  in the near future.

For Type 2, the potential efficiency of the PEM is assumed to be 74%, and the optical loss is assumed to be  $\approx 20\%$ . Given this positive value, the LCOH is  $\$7.14 \text{ kg}^{-1}$  for Type 2.<sup>[119]</sup> In addition, changes in concentrated PV, electrolyzer, and hard-BoS prices are significant. In the detailed distribution of the concentrated PV (the first bar in Figure 13b), apart from the III–V solar cell costs, the divided price of Fresnel lenses ( $\$1.37 \text{ kg}^{-1}$ ) accounts for a high proportion of the total cost. 3j III–V solar cell and Fresnel lens costs are expected to decrease with market expansion, and half of the current price ( $\$37$  and  $\$50$ , respectively) could be reached. As the electrolyzer components in Type

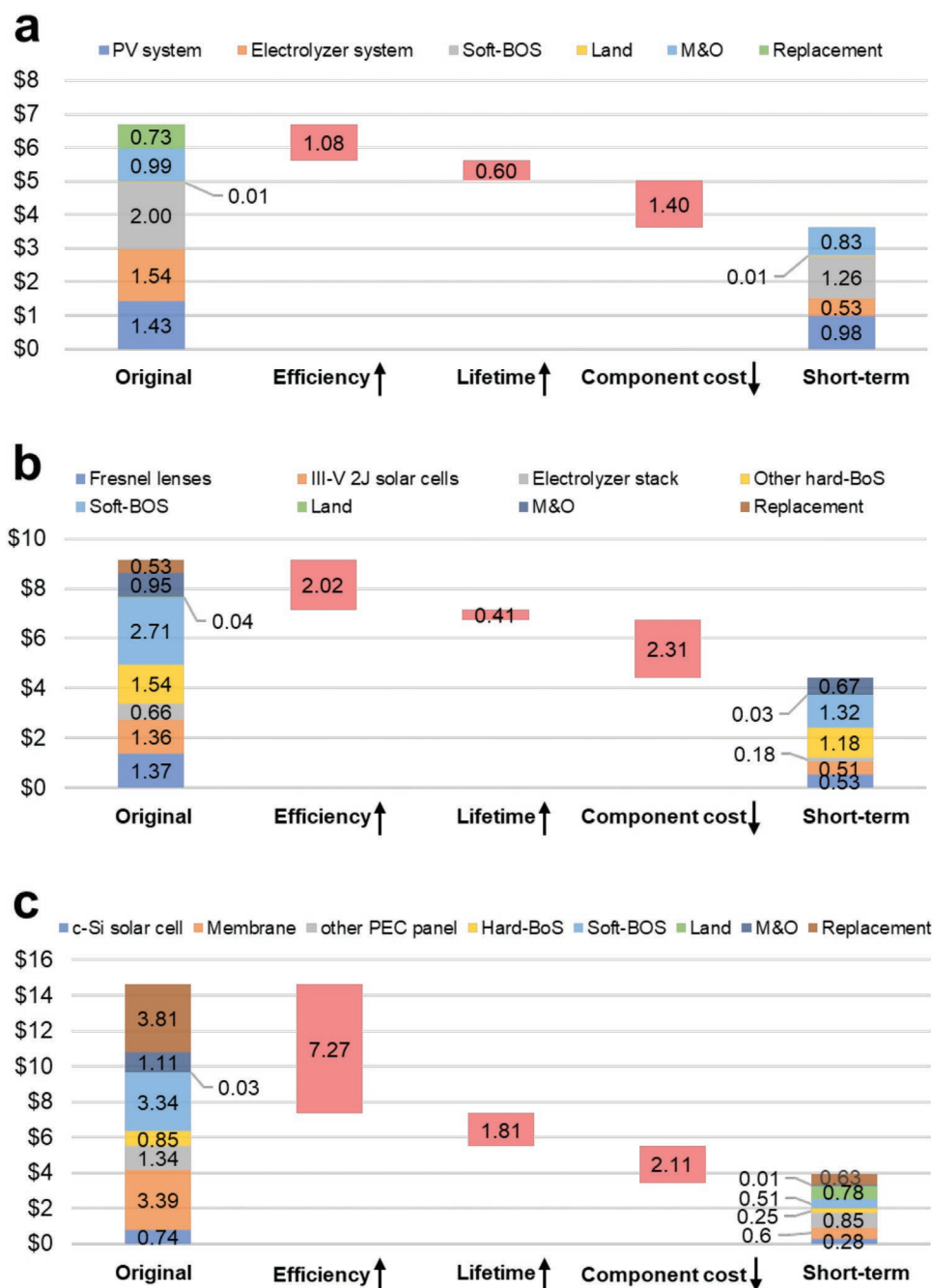


Figure 13. Waterfall charts showing the potential LCOH in the short term for: a) Type 1; b) Type 2; c) Type 3.

2 are similar to those in Type 1, the same price trend is assumed. Taking all these parameters into account, we estimated that the potential LCOH for Type 2 was reduced to  $\$4.42 \text{ kg}^{-1}$  (Figure 13b).

For Type 3 analysis, double improvement for the STH efficiency ( $\approx 13\%$ ) is positively estimated for future LCOH. This STH efficiency leads to a cost reduction of LCOH ( $\$7.33 \text{ kg}^{-1}$ ) even without the cost reduction of components. The lifetime for Type 3 is more sensitive than the other two systems. If a longer lifetime (more than 20 years) could be achieved, the LCOH would decrease to  $\$5.52 \text{ kg}^{-1}$ . Therefore, the future

development of PEC should still focus on pursuing higher STH efficiency and a longer lifetime. At the high performance, cost reduction of the main components may achieve the cost target. The most sensitive part of Type 3 in price is the PEC panels. Specifically, Figure 13c shows that the cost of Nafion membranes, p-Si solar cells, and TCO significantly contribute to the PEC panels. For Nafion membrane costs, we assume that  $\approx \$500 \text{ m}^{-2}$  is achievable, which is the potential cost of Nafion membranes in other techno-economic analyses.<sup>[3c,106a]</sup> For p-Si solar cells and TCO costs, there are few data about their cost, so a 20% decrease would be a reasonable assumption. As PEC

develops, the contingency cost will likely decrease from 30% to 15%, a typical value of mature technology.<sup>[106b]</sup> If all the assumptions mentioned above were realized, the LCOH for Type 3 could be \$3.41 kg<sup>-1</sup> (Figure 13c), which would be comparable to PV-EC. With a bolder prediction—the membrane cost is reduced to 10% of the current price (\$1000 m<sup>-2</sup>)—the LCOH (\$2.41) of PEC will dramatically exceed PV-EC (\$3.62) and be close to the final goal (\$2.00).

## 6. Summary and Outlook

PV-EC and PEC technologies have the potential for large-scale solar hydrogen production with a competitive cost. Solar hydrogen generation devices developed over 50 years are reviewed. The highest STH efficiencies are 8% (PEC-PEC), 12% (PEC-PV), 19% (buried junction PV), 30% (traditional PV-EC), and 16% (integrated PV-EC), and it progresses rapidly. High-efficiency devices usually have complex structures and expensive materials (multiple buried junctions III–V semiconductors), which are unlikely to meet TW energy challenges due to their prices and reserves. For PEC, the STH efficiency of simple structures (SLJ) and earth-abundant material-based devices are below 10%. A comparative techno-economic analysis of PV-EC and PEC systems was performed based on state-of-the-art demonstration to describe the economics of solar hydrogen production better. The results estimate the LCOH for traditional (Type 1) and integrated (Type 2) PV-EC of \$6.70 and \$9.16 kg<sup>-1</sup>, respectively. The LCOH for a PEC (Type 3) was \$14.60 kg<sup>-1</sup>. For the future perspective of a green hydrogen economy, we predict the LCOH of these three solar hydrogen systems while using optimistic assumptions in the short term. The results show a significant decrease in future LCOH as all three systems evolve, which provides direction for future research:

- 1) For Type 1, both PV and electrolyzer are available, and a large-scale plant can be constructed with current technology. In recent years, the number of demonstration projections and the capacity of traditional PV-EC hydrogen production systems have increased. For example, the FH2R project in Fukushima, Japan, has been finished.<sup>[126]</sup> The project combines a 20 MW solar power station with a 10 MW water electrolysis device, producing 1200 standard cubic meters of hydrogen per hour. Canada has built a “green hydrogen” plant with 20 MW capacity.<sup>[127]</sup> Besides, other countries have also announced plans for hundreds of megawatts of renewable electric energy projects within 10 years. These advancements indicate the practicality of traditional PV-EC. Our analysis shows that the construction and operating costs are higher than those of conventional fossil fuel-based methods.<sup>[22]</sup> Developing a PEM-electrolyzer system or other promising electrolysis technologies (with both higher efficiency and lower price) would be a priority to reduce LCOH.
- 2) The techno-economic analysis for Type 2 shows that LCOH could be \$9.12 kg<sup>-1</sup> with a concentrated and integrated configuration. Although Type 2 LCOH is more expensive than Type 1, further decreases may be expected with optimistic assumptions. Specifically, in addition to the PEM-electrolyzer system, the concentrated-PV system (Fresnel lenses and III–V

solar cells) should be well developed. Not only does the price reduction, but properties, such as transparency for Fresnel lenses and the ability to tolerate high concentrated solar irradiance, should be further improved.

- 3) Unlike the first two systems, Type 3 has a more straightforward configuration due to the spontaneous formation of SLJ. However, the photovoltage and photocurrent produced by SLJ are not high enough to construct a PEC on a large scale. Analysis indicates that PEC is unlikely to beat PV-EC based on the present perspective. However, PEC can potentially exceed PV-EC in the future for a straightforward process. New Earth-abundant semiconductors are needed to create effective SLJ with high STH efficiency and extend their stability. Over 10% of STH efficiency with stability similar to PV cells is necessary, which would decrease the cost of PEC panels and the replacement of the system. Advances achieve water splitting without PV technology assistance, eliminating the prohibitive cost for PV-based materials and complex wiring configurations. Finally, the cost of critical components, such as the Nafion membrane, should be further reduced. We estimate that by combining optimistic assumptions, PEC has a huge opportunity to outperform PV-EC in the future.

## Supporting Information

Supporting Information is available from the Wiley Online Library or from the author.

## Acknowledgements

This work was financially supported by the City University of Hong Kong funding (9380107).

## Conflict of Interest

The authors declare no conflict of interest.

## Keywords

electrolysis, hydrogen, photocatalysis, photoelectrochemistry, photovoltaics, solar energy

Received: September 3, 2022  
Revised: November 18, 2022  
Published online: January 8, 2023

- [1] a) I. Staffell, D. Scamman, A. V. Abad, P. Balcombe, P. E. Dodds, P. Ekins, N. Shah, K. R. Ward, *Energy Environ. Sci.* **2019**, *12*, 463; b) K. Espegren, S. Damman, P. Piscicella, I. Graabak, A. Tomasgard, *Int. J. Hydrogen Energy* **2021**, *46*, 23125; c) J. A. Turner, *Science* **2004**, *305*, 972.
- [2] a) J. Kibsgaard, I. Chorkendorff, *Nat. Energy* **2019**, *4*, 430; b) M. Ball, M. Wietschel, *Int. J. Hydrogen Energy* **2009**, *34*, 615.
- [3] a) P. Nikolaidis, A. Poullikkas, *Renewable Sustainable Energy Rev.* **2017**, *67*, 597; b) S. Ardo, D. F. Rivas, M. A. Modestino, V. S. Greiving, F. F. Abdi, E. Alarcon Llado, V. Artero, K. Ayers,

- C. Battaglia, J. P. Becker, D. Bederak, A. Berger, F. Buda, E. Chinello, B. Dam, V. Di Palma, T. Edvinsson, K. Fujii, H. Gardeniers, H. Geerlings, S. M. H. Hashemi, S. Haussener, F. Houle, J. Huskens, B. D. James, K. Konrad, A. Kudo, P. P. Kunturu, D. Lohse, B. Mei, et al., *Energy Environ. Sci.* **2018**, *11*, 2768; c) M. R. Shaner, H. A. Atwater, N. S. Lewis, E. W. McFarland, *Energy Environ. Sci.* **2016**, *9*, 2354.
- [4] a) M. Perez, R. Perez, *IEA SHC Newslett.* **2015**, *62*, 4; b) J. H. Kim, D. Hansora, P. Sharma, J. W. Jang, J. S. Lee, *Chem. Soc. Rev.* **2019**, *48*, 1908.
- [5] a) S. Tembhurne, F. Nandjou, S. Haussener, *Nat. Energy* **2019**, *4*, 399; b) M. A. Khan, I. Al-Shankiti, A. Ziani, N. Wehbe, H. Idriss, *Angew. Chem., Int. Ed. Engl.* **2020**, *59*, 14802; c) J. Jia, L. C. Seitz, J. D. Benck, Y. Huo, Y. Chen, J. W. Ng, T. Bilir, J. S. Harris, T. F. Jaramillo, *Nat. Commun.* **2016**, *7*, 13237; d) C. Moon, B. Seger, P. C. K. Vesborg, O. Hansen, I. Chorkendorff, *Cell Rep. Phys. Sci.* **2020**, *1*, 100261; e) Y. J. Wang, J. Schwartz, J. Gim, R. Hovden, Z. T. Mi, *ACS Energy Lett.* **2019**, *4*, 1541; f) H. C. Fu, P. Varadhan, C. H. Lin, J. H. He, *Nat. Commun.* **2020**, *11*, 3930.
- [6] A. J. Bard, M. A. Fox, *Acc. Chem. Res.* **1995**, *28*, 141.
- [7] S. Y. Reece, J. A. Hamel, K. Sung, T. D. Jarvi, A. J. Esswein, J. J. Pijpers, D. G. Nocera, *Science* **2011**, *334*, 645.
- [8] K. Welter, N. Hamzelui, V. Smirnov, J. P. Becker, W. Jaegermann, F. Finger, *J. Mater. Chem. A* **2018**, *6*, 15968.
- [9] a) A. Schneemann, J. L. White, S. Kang, S. Jeong, L. F. Wan, E. S. Cho, T. W. Heo, D. Prendergast, J. J. Urban, B. C. Wood, M. D. Allendorf, V. Stavila, *Chem. Rev.* **2018**, *118*, 10775; b) J. Andersson, S. Gronkvist, *Int. J. Hydrogen Energy* **2019**, *44*, 11901; c) D. A. Cullen, K. C. Neyerlin, R. K. Ahluwalia, R. Mukundan, K. L. More, R. L. Borup, A. Z. Weber, D. J. Myers, A. Kusoglu, *Nat. Energy* **2021**, *6*, 462.
- [10] N. S. Lewis, *Nature* **2001**, *414*, 589.
- [11] M. T. Mayer, *Curr. Opin. Electrochem.* **2017**, *2*, 104.
- [12] a) S. Chu, W. Li, Y. F. Yan, T. Hamann, I. Shih, D. W. Wang, Z. T. Mi, *Nano Futures* **2017**, *1*, 022001; b) K. Sivula, R. van de Krol, *Nat. Rev. Mater.* **2016**, *1*, 15010.
- [13] M. G. Walter, E. L. Warren, J. R. McKone, S. W. Boettcher, Q. Mi, E. A. Santori, N. S. Lewis, *Chem. Rev.* **2010**, *110*, 6446.
- [14] M. S. Prévot, K. Sivula, *J. Phys. Chem. C* **2013**, *117*, 17879.
- [15] a) D. G. Nocera, *Acc. Chem. Res.* **2012**, *45*, 767; b) P. Varadhan, H. C. Fu, Y. C. Kao, R. H. Horng, J. H. He, *Nat. Commun.* **2019**, *10*, 5282.
- [16] a) O. Khaselev, J. A. Turner, *Science* **1998**, *280*, 425; b) B. Koo, D. Kim, P. Boonmongkolras, S. R. Pae, S. Byun, J. Kim, J. H. Lee, D. H. Kim, S. Kim, B. T. Ahn, S. W. Nam, B. Shin, *ACS Appl. Energy Mater.* **2020**, *3*, 2296; c) V. Andrei, R. L. Z. Hoyer, M. Crespo-Quesada, M. Bajada, S. Ahmad, M. De Volder, R. Friend, E. Reisner, *Adv. Energy Mater.* **2018**, *8*, 1801403.
- [17] V. Cristino, S. Berardi, S. Caramori, R. Argazzi, S. Carli, L. Meda, A. Tacca, C. A. Bignozzi, *Phys. Chem. Chem. Phys.* **2013**, *15*, 13083.
- [18] a) S. Licht, B. Wang, S. Mukerji, T. Soga, M. Umeno, H. Tributsch, *Int. J. Hydrogen Energy* **2001**, *26*, 653; b) F. Katsushi, N. Shinichiro, W. Kentaroh, B. Behgol, S. Masakazu, N. Yoshiaki, *Mater. Res. Soc. Symp. Proc.* **2013**, *1491*, c1106; c) J. Gao, F. Sahli, C. J. Liu, D. Ren, X. Y. Guo, J. Werner, Q. Jeangros, S. M. Zakeeruddin, C. Ballif, M. Gratzel, J. S. Luo, *Joule* **2019**, *3*, 2930.
- [19] a) J. S. Luo, J. H. Im, M. T. Mayer, M. Schreier, M. K. Nazeeruddin, N. G. Park, S. D. Tilley, H. J. Fan, M. Gratzel, *Science* **2014**, *345*, 1593; b) J.-W. Schuttauf, M. A. Modestino, E. Chinello, D. Lambelet, A. Delfino, D. Domine, A. Faes, M. Despeisse, J. Bailat, D. Psaltis, C. Moser, C. Ballifa, *J. Electrochem. Soc.* **2016**, *163*, F1177.
- [20] A. C. Nielander, M. R. Shaner, K. M. Papadantonakis, S. A. Francis, N. S. Lewis, *Energy Environ. Sci.* **2015**, *8*, 16.
- [21] M. Dumortier, S. Tembhurne, S. Haussener, *Energy Environ. Sci.* **2015**, *8*, 3614.
- [22] B. A. Pinaud, J. D. Benck, L. C. Seitz, A. J. Forman, Z. B. Chen, T. G. Deutsch, B. D. James, K. N. Baum, G. N. Baum, S. Ardo, H. L. Wang, E. Miller, T. F. Jaramillo, *Energy Environ. Sci.* **2013**, *6*, 1983.
- [23] J. L. Young, M. A. Steiner, H. Doscher, R. M. France, J. A. Turner, T. G. Deutsch, *Nat. Energy* **2017**, *2*, 17028.
- [24] C. R. C. Mark, T. Winkler, D. G. Nocera, T. Buonassisi, *Proc. Natl. Acad. Sci. U. S. A.* **2013**, *110*, E1076.
- [25] W. J. Chang, K. H. Lee, H. Ha, K. Jin, G. Kim, S. T. Hwang, H. M. Lee, S. W. Ahn, W. Yoon, H. Seo, J. S. Hong, Y. K. Go, J. I. Ha, K. T. Nam, *ACS Omega* **2017**, *2*, 1009.
- [26] S. Hu, C. X. Xiang, S. Haussener, A. D. Berger, N. S. Lewis, *Energy Environ. Sci.* **2013**, *6*, 2984.
- [27] F. Urbain, V. Smirnov, J. P. Becker, U. Rau, J. Ziegler, F. Yang, B. Kaiser, W. Jaegermann, S. Hoch, M. Blug, F. Finger, *Chem. Phys. Lett.* **2015**, *638*, 25.
- [28] E. N. Costogoe, R. K. Yasu, *Sol. Energy* **1977**, *19*, 205.
- [29] T. L. Gibson, N. A. Kelly, *Int. J. Hydrogen Energy* **2008**, *33*, 5931.
- [30] a) N. A. Kelly, T. L. Gibson, D. B. Ouwkerk, *Int. J. Hydrogen Energy* **2008**, *33*, 2747; b) N. A. Kelly, T. L. Gibson, *Sol. Energy* **2009**, *83*, 2092; c) T. L. Gibson, N. A. Kelly, *Int. J. Hydrogen Energy* **2010**, *35*, 900; d) N. A. Kelly, T. L. Gibson, M. Cai, J. A. Spearot, D. B. Ouwkerk, *Int. J. Hydrogen Energy* **2010**, *35*, 892; e) N. A. Kelly, T. L. Gibson, *Sol. Energy* **2011**, *85*, 111; f) N. A. Kelly, T. L. Gibson, D. B. Ouwkerk, *Int. J. Hydrogen Energy* **2011**, *36*, 15803.
- [31] C. R. Cox, J. Z. Lee, D. G. Nocera, T. Buonassisi, *Proc. Natl. Acad. Sci. U. S. A.* **2014**, *111*, 14057.
- [32] H. Chen, L. Song, S. Ouyang, J. Wang, J. Lv, J. Ye, *Adv. Sci.* **2019**, *6*, 1900465.
- [33] X. Yi, L. Song, S. Ouyang, N. Wang, H. Chen, J. Wang, J. Lv, J. Ye, *Small* **2021**, *17*, 2102222.
- [34] J. Tournet, Y. Lee, S. K. Krishna, H. H. Tan, C. Jagadish, *ACS Energy Lett.* **2020**, *5*, 611.
- [35] Y. Wang, A. Sharma, T. Duong, H. Arandiyana, T. Zhao, D. Zhang, Z. Su, M. Garbrecht, F. J. Beck, S. Karuturi, C. Zhao, K. Catchpole, *Adv. Energy Mater.* **2021**, *11*, 2101053.
- [36] a) K. Fujii, S. Nakamura, M. Sugiyama, K. Watanabe, B. Bagheri, Y. Nakano, *Int. J. Hydrogen Energy* **2013**, *38*, 14424; b) M. Sugiyama, A. Nakamura, K. Watanabe, Y. Ota, K. Nishioka, Y. Nakano, K. Fujii, in *2015 IEEE 42nd Photovoltaic Specialist Conf. (PVSC)*, (Ed. A. Freundlich) IEEE, Piscataway, NJ **2015**, pp. 1–4; c) A. Nakamura, Y. Ota, K. Koike, Y. Hidaka, K. Nishioka, M. Sugiyama, K. Fujii, *Appl. Phys. Express* **2015**, *8*, 107101; d) Y. Ota, D. Yamashita, H. Nakao, Y. Yonezawa, Y. Nakashima, H. Ebe, M. Inagaki, R. Mikami, Y. Abiko, T. Iwasaki, M. Sugiyama, K. Nishioka, *Appl. Phys. Express* **2018**, *11*, 077101; e) Y. O. Soe, H. Wai, D. Yamashita, M. Sugiyama, K. Nishioka, in *Grand Renewable Energy 2018 Int. Conf. Exhibition*, J-STAGE, Pacifico Yokohama, Japan, **2018**.
- [37] C. W. Huang, C. H. Liao, C. H. Wu, J. C. S. Wu, *Sol. Energy Mater. Sol. Cells* **2012**, *107*, 322.
- [38] S. A. Bonke, M. Wiechen, D. R. MacFarlane, L. Spiccia, *Energy Environ. Sci.* **2015**, *8*, 2791.
- [39] S. H. Hsu, J. Miao, L. Zhang, J. Gao, H. Wang, H. Tao, S. F. Hung, A. Vasileff, S. Z. Qiao, B. Liu, *Adv. Mater.* **2018**, *30*, 1707261.
- [40] M. A. Khan, I. Al-Shankiti, A. Ziani, H. Idriss, *Sustainable Energy Fuels* **2021**, *5*, 1085.
- [41] a) Y. Li, H. Xie, E. L. Lim, A. Hagfeldt, D. Bi, *Adv. Energy Mater.* **2021**, *12*, 2102730; b) M. A. Mahmud, T. Duong, J. Peng, Y. Wu, H. Shen, D. Walter, H. T. Nguyen, N. Mozaffari, G. D. Tabi, K. R. Catchpole, K. J. Weber, T. P. White, *Adv. Funct. Mater.* **2021**,

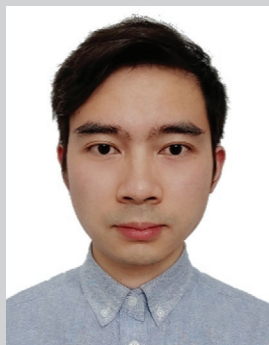
- 32, 2009164; c) R. Wang, M. Mujahid, Y. Duan, Z. K. Wang, J. Xue, Y. Yang, *Adv. Funct. Mater.* **2019**, *29*, 1808843
- [42] L. B. Ma, W. J. Zhang, P. Y. Zhao, J. Liang, Y. Hu, G. Y. Zhu, R. P. Chen, Z. X. Tie, J. Liu, Z. Jin, *J. Mater. Chem. A* **2018**, *6*, 20076.
- [43] J. S. Luo, D. A. Vermaas, D. Q. Bi, A. Hagfeldt, W. A. Smith, M. Gratzel, *Adv. Energy Mater.* **2016**, *6*, 1600100.
- [44] S. Pan, R. Li, Q. Zhang, C. Cui, M. Wang, B. Shi, P. Wang, C. Zhang, B. Zhang, Y. Zhao, X. Zhang, *J. Mater. Chem. A* **2021**, *9*, 14085.
- [45] N. G. Dhere, A. H. Jahagirdar, *Thin Solid Films* **2005**, *480*, 462.
- [46] T. J. Jacobsson, V. Fjallstrom, M. Sahlberg, M. Edoff, T. Edvinsson, *Energy Environ. Sci.* **2013**, *6*, 3676.
- [47] S. Esiner, H. van Eersel, M. M. Wienk, R. A. Janssen, *Adv. Mater.* **2013**, *25*, 2932.
- [48] N. S. Lewis, *Science* **2016**, *351*, 353.
- [49] a) X. Elias, Q. Liu, C. Gimbert-Surinach, R. Matheu, P. Mantilla-Perez, A. Martinez-Otero, X. Sala, J. Martorell, A. Llobet, *ACS Catal.* **2016**, *6*, 3310; b) S. Esiner, H. van Eersel, G. W. van Pruissen, M. Turbiez, M. M. Wienk, R. A. Janssen, *ACS Appl. Mater. Interfaces* **2016**, *8*, 26972; c) S. Esiner, G. W. P. van Pruissen, M. M. Wienk, R. A. J. Janssen, *J. Mater. Chem. A* **2016**, *4*, 5107; d) Y. Gao, V. M. Le Corre, A. Gaitis, M. Neophytou, M. A. Hamid, K. Takanabe, P. M. Beaujuge, *Adv. Mater.* **2016**, *28*, 3366; e) Q. Wu, J. Guo, R. Sun, J. Guo, S. Jia, Y. Li, J. Wang, J. Min, *Nano Energy* **2019**, *61*, 559; f) Y. K. Kim, T. H. Lee, J. Yeop, W. J. Byun, J. H. Kim, J. Y. Kim, J. S. Lee, *Appl. Catal., B* **2022**, *309*, 121237.
- [50] O. J. Murphy, J. O. Bockris, *Int. J. Hydrogen Energy* **1984**, *9*, 557.
- [51] R. E. Rocheleau, E. L. Miller, A. Misra, *Energy Fuels* **1998**, *12*, 3.
- [52] O. Khaselev, A. Bansal, J. A. Turner, *Int. J. Hydrogen Energy* **2001**, *26*, 127.
- [53] F. Dimroth, G. Peharz, U. Wittstadt, B. Hacker, A. W. Bett, in *2006 IEEE 4th World Conf. Photovolt. Energy Conf.*, (Ed: N. D. Stojadinovic) IEEE, Piscataway, NJ **2006**, pp. 640–643.
- [54] G. Peharz, F. Dimroth, U. Wittstadt, *Int. J. Hydrogen Energy* **2007**, *32*, 3248.
- [55] a) J. Ohlmann, J. F. M. Sanchez, D. Lackner, P. Förster, M. Steiner, A. Fallisch, F. Dimroth, *AIP Conf. Proc.* **2016**, *1766*, 080004; b) A. Fallisch, L. Schellhase, J. Fresko, M. Zechmeister, M. Zedda, J. Ohlmann, L. Zielke, N. Paust, T. Smolinka, *Int. J. Hydrogen Energy* **2017**, *42*, 13544.
- [56] A. Fallisch, L. Schellhase, J. Fresko, M. Zedda, J. Ohlmann, M. Steiner, A. Bosch, L. Zielke, S. Thiele, F. Dimroth, T. Smolinka, *Int. J. Hydrogen Energy* **2017**, *42*, 26804.
- [57] S. Rau, S. Vierrath, J. Ohlmann, A. Fallisch, D. Lackner, F. Dimroth, T. Smolinka, *Energy Technol.* **2014**, *2*, 43.
- [58] J. Ziegler, B. Kaiser, W. Jaegermann, F. Urbain, J. P. Becker, V. Smirnov, F. Finger, *ChemPhysChem* **2014**, *15*, 4026.
- [59] F. Urbain, V. Smirnov, J. P. Becker, U. Rau, J. Ziegler, B. Kaiser, W. Jaegermann, F. Finger, *Sol. Energy Mater. Sol. Cells* **2015**, *140*, 275.
- [60] J. P. Becker, F. Urbain, V. Smirnov, U. Rau, J. Ziegler, B. Kaiser, W. Jaegermann, F. Finger, *Phys. Status Solidi A* **2016**, *213*, 1738.
- [61] F. Urbain, V. Smirnov, J. P. Becker, A. Lambertz, F. Yang, J. Ziegler, B. Kaiser, W. Jaegermann, U. Rau, F. Finger, *Energy Environ. Sci.* **2016**, *9*, 145.
- [62] B. Turan, J. P. Becker, F. Urbain, F. Finger, U. Rau, S. Haas, *Nat. Commun.* **2016**, *7*, 12681.
- [63] M. N. Lee, B. Turan, J. P. Becker, K. Welter, B. Klingebiel, E. Neumann, Y. J. Sohn, T. Merdzhanova, T. Kirchartz, F. Finger, U. Rau, S. Haas, *Adv. Sustainable Syst.* **2020**, *4*, 2000070.
- [64] J. P. Becker, B. Turan, V. Smirnov, K. Welter, F. Urbain, J. Wolff, S. Haas, F. Finger, *J. Mater. Chem. A* **2017**, *5*, 4818.
- [65] I. B. Pehlivan, J. Oscarsson, Z. Qiu, L. Stolt, M. Edoff, T. Edvinsson, *iScience* **2021**, *24*, 101910.
- [66] A. Fujishima, K. Honda, *Nature* **1972**, *238*, 37.
- [67] P. Peerakiatkhajohn, J.-H. Yun, S. Wang, L. Wang, *J. Photonics Energy* **2016**, *7*, 012006.
- [68] K. Ohasht, J. McCann, J. O'M. Bockris, *Nature* **1977**, *266*, 610.
- [69] G. K. Mor, O. K. Varghese, R. H. T. Wilke, S. Sharma, K. Shankar, T. J. Latempa, K.-S. Choi, C. A. Grimes, *Nano Lett.* **2008**, *8*, 1906.
- [70] S. Ida, K. Yamada, T. Matsunaga, H. Hagiwara, Y. Matsumoto, T. Ishihara, *J. Am. Chem. Soc.* **2010**, *132*, 17343.
- [71] C. Liu, J. Tang, H. M. Chen, B. Liu, P. Yang, *Nano Lett.* **2013**, *13*, 2989.
- [72] R. C. Kainthla, B. Zelenay, J. O. Bockris, *J. Electrochem. Soc.* **1987**, *134*, 841.
- [73] J. W. Ager, M. R. Shaner, K. A. Walczak, I. D. Sharp, S. Ardo, *Energy Environ. Sci.* **2015**, *8*, 2811.
- [74] J. H. Kim, J. S. Lee, *Adv. Mater.* **2019**, *31*, 1806938.
- [75] a) I. V. Bagal, N. R. Chodankar, M. A. Hassan, A. Waseem, M. A. Johar, D. H. Kim, S. W. Ryu, *Int. J. Hydrogen Energy* **2019**, *44*, 21351; b) Q. Chen, G. Z. Fan, H. W. Fu, Z. S. Li, Z. G. Zou, *Adv. Phys. X* **2018**, *3*, 864.
- [76] A. Paracchino, V. Laporte, K. Sivula, M. Gratzel, E. Thimsen, *Nat. Mater.* **2011**, *10*, 456.
- [77] P. Borno, F. F. Abdi, S. D. Tilley, B. Dam, R. van de Krol, M. Graetzel, K. Sivula, *J. Phys. Chem. C* **2014**, *118*, 16959.
- [78] L. F. Pan, J. H. Kim, M. T. Mayer, M. K. Son, A. Ummadisingu, J. S. Lee, A. Hagfeldt, J. S. Luo, M. Gratzel, *Nat. Catal.* **2018**, *1*, 412.
- [79] Y. Zhang, H. Lv, Z. Zhang, L. Wang, X. Wu, H. Xu, *Adv. Mater.* **2021**, *33*, 2008264.
- [80] S. Ye, W. Shi, Y. Liu, D. Li, H. Yin, H. Chi, Y. Luo, N. Ta, F. Fan, X. Wang, C. Li, *J. Am. Chem. Soc.* **2021**, *143*, 12499.
- [81] J. W. Jang, C. Du, Y. Ye, Y. Lin, X. Yao, J. Thorne, E. Liu, G. McMahon, J. Zhu, A. Javey, J. Guo, D. Wang, *Nat. Commun.* **2015**, *6*, 7447.
- [82] a) D. Shao, Y. Cheng, J. He, D. Feng, L. Zheng, L. Zheng, X. Zhang, J. Xu, W. Wang, W. Wang, F. Lu, H. Dong, L. Li, H. Liu, R. Zheng, H. Liu, *ACS Catal.* **2017**, *7*, 5308; b) W. Shi, D. Li, W. Fan, J. Ma, C. Li, W. Yu, J. Shi, C. Li, *Adv. Funct. Mater.* **2020**, *30*, 2003399.
- [83] Y. Pihosh, I. Turkevych, K. Mawatari, J. Uemura, Y. Kazoe, S. Kosar, K. Makita, T. Sugaya, T. Matsui, D. Fujita, M. Tosa, M. Kondo, T. Kitamori, *Sci. Rep.* **2015**, *5*, 11141.
- [84] F. F. Abdi, L. Han, A. H. Smets, M. Zeman, B. Dam, R. van de Krol, *Nat. Commun.* **2013**, *4*, 2195.
- [85] J. H. Kim, J. W. Jang, Y. H. Jo, F. F. Abdi, Y. H. Lee, R. van de Krol, J. S. Lee, *Nat. Commun.* **2016**, *7*, 13380.
- [86] Y. Qiu, W. Liu, W. Chen, W. Chen, G. Zhou, P. C. Hsu, R. Zhang, Z. Liang, S. Fan, Y. Zhang, Y. Cui, *Sci. Adv.* **2016**, *2*, e1501764.
- [87] S. E. Jun, S. P. Hong, S. Choi, C. Kim, S. G. Ji, I. J. Park, S. A. Lee, J. W. Yang, T. H. Lee, W. Sohn, J. Y. Kim, H. W. Jang, *Small* **2021**, *17*, 2103457.
- [88] J. Brillet, J. H. Yum, M. Cornuz, T. Hisatomi, R. Solarska, J. Augustynski, M. Graetzel, K. Sivula, *Nat. Photonics* **2012**, *6*, 824.
- [89] a) K. Shin, J. B. Yoo, J. H. Park, *J. Power Sources* **2013**, *225*, 263; b) X. Shi, H. Jeong, S. J. Oh, M. Ma, K. Zhang, J. Kwon, I. T. Choi, I. Y. Choi, H. K. Kim, J. K. Kim, J. H. Park, *Nat. Commun.* **2016**, *7*, 11943.
- [90] a) B. Sun, T. Shi, Z. Liu, Z. Tang, J. Zhou, G. Liao, *RSC Adv.* **2016**, *6*, 110120; b) X. Zhang, B. Zhang, K. Cao, J. Brillet, J. Chen, M. Wang, Y. Shen, *J. Mater. Chem. A* **2015**, *3*, 21630.
- [91] Gurudayal, R. A. John, P. P. Boix, C. Yi, C. Shi, M. C. Scott, S. A. Veldhuis, A. M. Minor, S. M. Zakeeruddin, L. H. Wong, M. Graetzel, N. Mathews, *ChemPhysChem* **2017**, *10*, 2449.
- [92] J. H. Kim, Y. Jo, J. H. Kim, J. W. Jang, H. J. Kang, Y. H. Lee, D. S. Kim, Y. Jun, J. S. Lee, *ACS Nano* **2015**, *9*, 11820.
- [93] S. Wang, P. Chen, Y. Bai, J. H. Yun, G. Liu, L. Wang, *Adv. Mater.* **2018**, *30*, 1800486.

- [94] M. Kim, B. Lee, H. Ju, J. Y. Kim, J. Kim, S. W. Lee, *Adv. Mater.* **2019**, 31, 1903316.
- [95] G. H. Lin, M. Kapur, R. C. Kainthla, J. O. Bockris, *Appl. Phys. Lett.* **1989**, 55, 386.
- [96] J. Jin, K. Walczak, M. R. Singh, C. Karp, N. S. Lewis, C. X. Xiang, *Energy Environ. Sci.* **2014**, 7, 3371.
- [97] M. M. May, H. J. Lewerenz, D. Lackner, F. Dimroth, T. Hannappel, *Nat. Commun.* **2015**, 6, 8286.
- [98] W. H. Cheng, M. H. Richter, M. M. May, J. Ohlmann, D. Lackner, F. Dimroth, T. Hannappel, H. A. Atwater, H. J. Lewerenz, *ACS Energy Lett.* **2018**, 3, 1795.
- [99] E. Verlage, S. Hu, R. Liu, R. J. R. Jones, K. Sun, C. X. Xiang, N. S. Lewis, H. A. Atwater, *Energy Environ. Sci.* **2015**, 8, 3166.
- [100] S. Okamoto, M. Deguchi, S. Yotsuhashi, *J. Phys. Chem. C* **2017**, 121, 1393.
- [101] S. Esiner, R. E. M. Willems, A. Furlan, W. W. Li, M. M. Wienk, R. A. J. Janssen, *J. Mater. Chem. A* **2015**, 3, 23936.
- [102] J. Luo, Z. Li, S. Nishiwaki, M. Schreier, M. T. Mayer, P. Cendula, Y. H. Lee, K. Fu, A. Cao, M. K. Nazeeruddin, Y. E. Romanyuk, S. Buecheler, S. D. Tilley, L. H. Wong, A. N. Tiwari, M. Grätzel, *Adv. Energy Mater.* **2015**, 5, 1501520.
- [103] S. K. Karuturi, H. P. Shen, A. Sharma, F. J. Beck, P. Varadhan, T. Duong, P. R. Narangari, D. D. Zhang, Y. M. Wan, J. H. He, H. H. Tan, C. Jagadish, K. Catchpole, *Adv. Energy Mater.* **2020**, 10, 2000772.
- [104] W. Yang, J. Park, H.-C. Kwon, O. S. Hutter, L. J. Phillips, J. Tan, H. Lee, J. Lee, S. D. Tilley, J. D. Major, J. Moon, *Energy Environ. Sci.* **2020**, 13, 4362.
- [105] B. Eftekharinia, H. Pezeshki, A. Dabirian, *ACS Appl. Mater. Interfaces* **2020**, 12, 17424.
- [106] a) A. Grimm, W. A. de Jong, G. J. Kramer, *Int. J. Hydrogen Energy* **2020**, 45, 22545; b) M. S. Victoria Garcia, Pieter, Delft University of Technology, PDEng (post-Master) Individual Design Project Report **2015**.
- [107] a) C. A. Rodriguez, M. A. Modestino, D. Psaltis, C. Moser, *Energy Environ. Sci.* **2014**, 7, 3828; b) W. A. d. B. Jong, *Master Thesis*, Utrecht University, xx xx **2018**.
- [108] T. Maeda, H. Ito, Y. Hasegawa, Z. M. Zhou, M. Ishida, *Int. J. Hydrogen Energy* **2012**, 37, 4819.
- [109] M. A. Green, E. D. Dunlop, J. Hohl-Ebinger, M. Yoshita, N. Kopidakis, X. Hao, *Prog. Photovoltaics* **2021**, 29, 657.
- [110] M. A. Green, E. D. Dunlop, J. Hohl-Ebinger, M. Yoshita, N. Kopidakis, X. Hao, *Prog. Photovoltaics* **2021**, 30, 3.
- [111] EnergyTrend, <https://www.energytrend.com/solar-price.html> (accessed: May 2022).
- [112] A. Perea, C. Smith, M. Davis, X. Sun, B. White, M. Cox, G. Curtin, S. Rumery, R. Goldstein, C. Silver, J. Baca, the Solar Energy Industries Association (SEIA) and Wood Mackenzie, **2020**.
- [113] A. Christensen, The International Council on Clean Transportation, Consultant Report, June 4 **2020**, <https://theicct.org/publication/assessment-of-hydrogen-production-costs-from-electrolysis-united-states-and-europe/>.
- [114] A. Mayyas, M. Ruth, B. Pivovar, G. Bender, K. Wipke, NREL, (US DOE Contract no. AC36-08GO28308), Golden, CO, **2018**, <https://doi.org/10.2172/1557965>.
- [115] W. G. Colella, B. D. James, J. M. Moton, G. Saur, T. Ramsden, Electrolytic Hydrogen Production Workshop, NREL, Golden, CO, February **2014**, <https://www.energy.gov/eere/fuelcells/downloads/electrolytic-hydrogen-production-workshop>.
- [116] Land of America, <https://www.landsofamerica.com/property/23.41-acres-in-San-Bernardino-County-California/13418514/> (accessed: May 2022).
- [117] B. D. James, G. N. Baum, J. Perez, K. N. Baum, Directed Technologies Inc., (US DOE Contract no. GS-10F-009J), Arlington, VA **2009**.
- [118] United States Average Hourly Earnings, <https://tradingeconomics.com/united-states/average-hourly-earnings> (accessed: May 2022).
- [119] T. R. Kelsey, A. W. Horowitz, B. Smith, A. Ptak, NREL, (US DOE Contract no. AC36-08GO28308) **2018**, <https://doi.org/10.2172/1484349>.
- [120] <https://szhaiwang.en.made-in-china.com/product/tSjnkRorbycU/China-1010-1010mm-Foculs-1000mm-Sog-Linear-Fresnel-Lenses-for-Cpv-System.html> (accessed: September 2022).
- [121] Trading Economics-Copper, <https://tradingeconomics.com/commodity/copper> (accessed: May 2022).
- [122] Solar Tracking System Dual Axis, [https://www.alibaba.com/product-detail/Automatic-PV-2-Axis-Solar-Panel\\_1600150508500.html?spm=a2700.7724857.normal\\_offer.d\\_title.6b5087dbeXtgXZ&s=p&fullFirstScreen=true](https://www.alibaba.com/product-detail/Automatic-PV-2-Axis-Solar-Panel_1600150508500.html?spm=a2700.7724857.normal_offer.d_title.6b5087dbeXtgXZ&s=p&fullFirstScreen=true) (accessed: May 2022).
- [123] a) H. Döscher, J. L. Young, J. F. Geisz, J. A. Turner, T. G. Deutsch, *Energy Environ. Sci.* **2016**, 9, 74; b) H. Döscher, J. F. Geisz, T. G. Deutsch, J. A. Turner, *Energy Environ. Sci.* **2014**, 7, 2951.
- [124] M. A. Green, E. D. Dunlop, J. Hohl-Ebinger, M. Yoshita, N. Kopidakis, X. Hao, *Prog. Photovoltaics* **2020**, 28, 629.
- [125] D. Peterson, J. Vickers, D. DeSantis, U.S. Department of Energy, DOE Hydrogen Fuel Cells Program Record 19009, **2020**.
- [126] The World's Largest-Class Hydrogen Production, Fukushima Hydrogen Energy Research Field (FH2R) now is completed at Namie town in Fukushima, [https://www.toshiba-energy.com/en/info/info2020\\_0307.htm](https://www.toshiba-energy.com/en/info/info2020_0307.htm) (accessed: May 2022).
- [127] World's Largest Green-Hydrogen Plant inaugurated in Canada by Air Liquide, <https://www.rechargenews.com/transition/worlds-largest-green-hydrogen-plant-inaugurated-in-canada-by-air-liquide/2-1-952085> (accessed: May 2022).



**Zhongxiao LI** is pursuing his Ph.D. degree (2020 onward) under the supervision of Prof. Jr-Hau He at Department of Materials Science and Engineering at City University of Hong Kong, Hong Kong. He obtained his Bachelor's and Master's degree in Materials Science and Engineering from Tianjin University, China. His current research focuses on projects about the design of photoelectrochemical devices and scale-up to large-scale systems for solar fuels.





**Shi Fang** is a Ph.D. student in the research group of Prof. Haiding Sun at University of Science and Technology of China. Currently he has published more than 20 papers in peer-reviewed SCI-indexed journals with first-author paper in Nature Communications, Advanced Functional Materials, etc. His main research interests focus on gallium nitride (GaN) optoelectronic devices and metal organic chemical vapor deposition (MOCVD) epitaxy.



**Haiding Sun** received his Ph.D. in Electrical Engineering from Boston University. He is currently a professor at University of Science and Technology of China. He has published more than 100 papers in peer-reviewed SCI-indexed journals including Nature Electronics, Advanced Functional Materials, Nano Letters, etc. He has written 4 book chapters and holds 20+ patents. His research interests include the investigation of the molecular-beam epitaxy and MOCVD epitaxy, and fabrication and characterization of semiconductor materials for both optoelectronics and electronic devices.



**Ren-Jei Chung** is a professor in the Department of Chemical Engineering and Biotechnology at the National Taipei University of Technology (Taipei Tech), and also serves as the Director of the Advanced Materials Research Center. He received his B.S. (1999), M.S. (2001), and Ph.D. (2006) degrees in the Department of Materials Science and Engineering at National Tsing Hua University, Taiwan. He is awarded the Fellow of the Royal Society of Chemistry, and has his research interests in biomaterials, biomedical applications of nanotechnology, tissue engineering, and biosensors.



**Xiaosheng Fang** is currently a professor in the Department of Materials Science, Fudan University, China. He received his Ph.D. degree from the Institute of Solid State Physics (ISSP), Chinese Academy of Sciences in 2006. After then, he was JSPS postdoctoral fellow and research scientist at the National Institute for Materials Science, Japan. He was a visiting scholar at MIT and Harvard University in 2009 and 2016, respectively. His current research topic mainly focuses on inorganic semiconductors and their applications.



**Jr-Hau He** is the professor in Department of Materials Science and Engineering at City University of Hong Kong. He has been an influential scientist in optoelectronics and materials. He has made a major contribution to understanding light–mater interaction, which reflects on his achievement of photon management on the light harvesting devices. The nanotechnology he has developed has been transferred constantly to energy and light-emitting diode industry over the world. He was selected as Highly Cited Researchers (2020–2022, Clarivate’s Web of Science). He is a Fellow of OSA, RSC, and SPIE.